INSTRUMENTS AND METHODS OF INVESTIGATION

PACS numbers: 32.80.Rm, 42.82.Cr, **61.46.–w**, **68.65.–k**, **81.20.–n**

3D printing methods for micro- and nanostructures

K B Fritzler, V Ya Prinz

DOI: https://doi.org/10.3367/UFNe.2017.11.038239

Osamu Katagiri-Tanaka
A01212611@itesm.mx

20 May 2020

K.B. Fritzler, V.Y. Prinz, 3D printing methods for micro- and nanostructures, Uspekhi Fiz. Nauk. 189 (2019) 55–71. https://doi.org/10.3367/UFNr.2017.11.038239.

Nanostereolithography (Charles Hull, 1986)

Is one of the earliest and most popular additive manufacturing methods by layer-by-layer formation of 3D objects by photoirradiation.

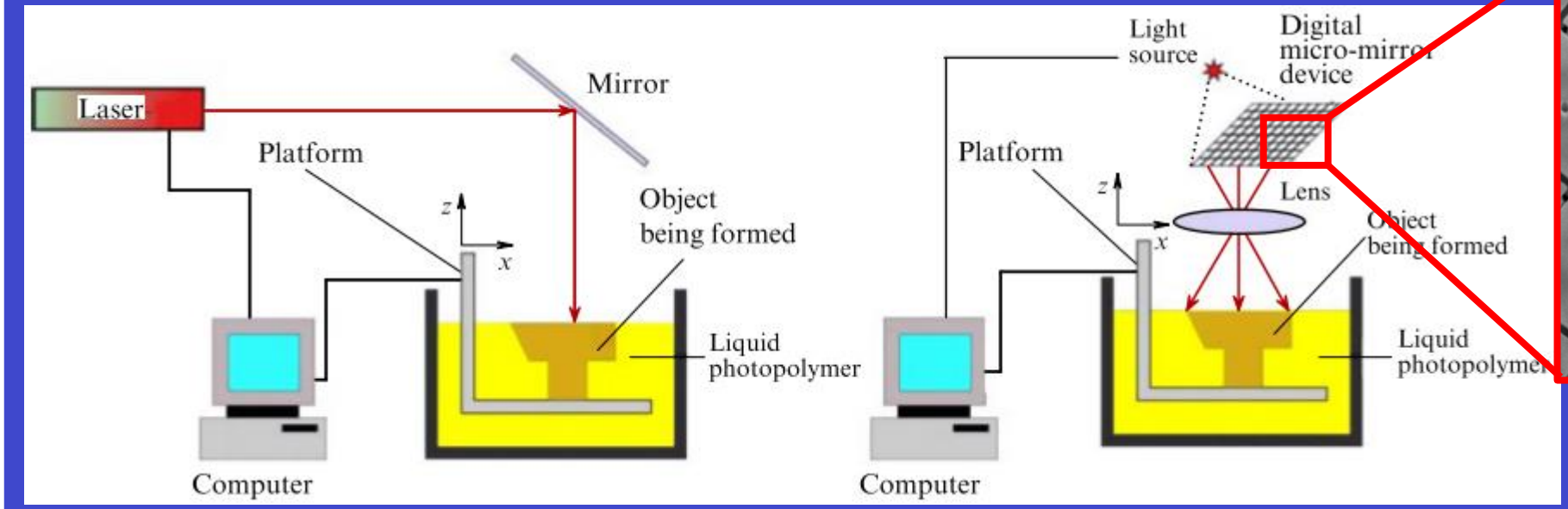

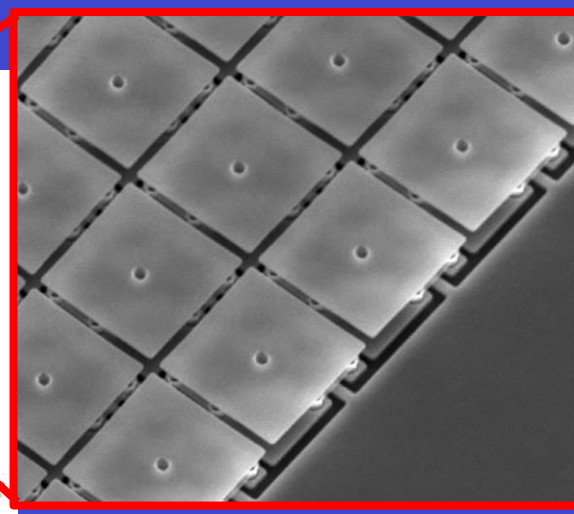

10 by 10 μm mirrors

scanning stereolithography (point-by-point solidification)

projection stereolithography (layer-by-layer solidification)

How Digital Light Processing (DLP) works - YouTube, (n.d.). https://www.youtube.com/watch?v=9nb8mM3uEIc (accessed 20 May 2020).
Hull C W, U.S. Patent No. 4575330A (1986)

Two-photon polymerization (Maruo, 1997)

Enhancing the resolution of stereolithographic methods to about 1/100 the optical wave-length

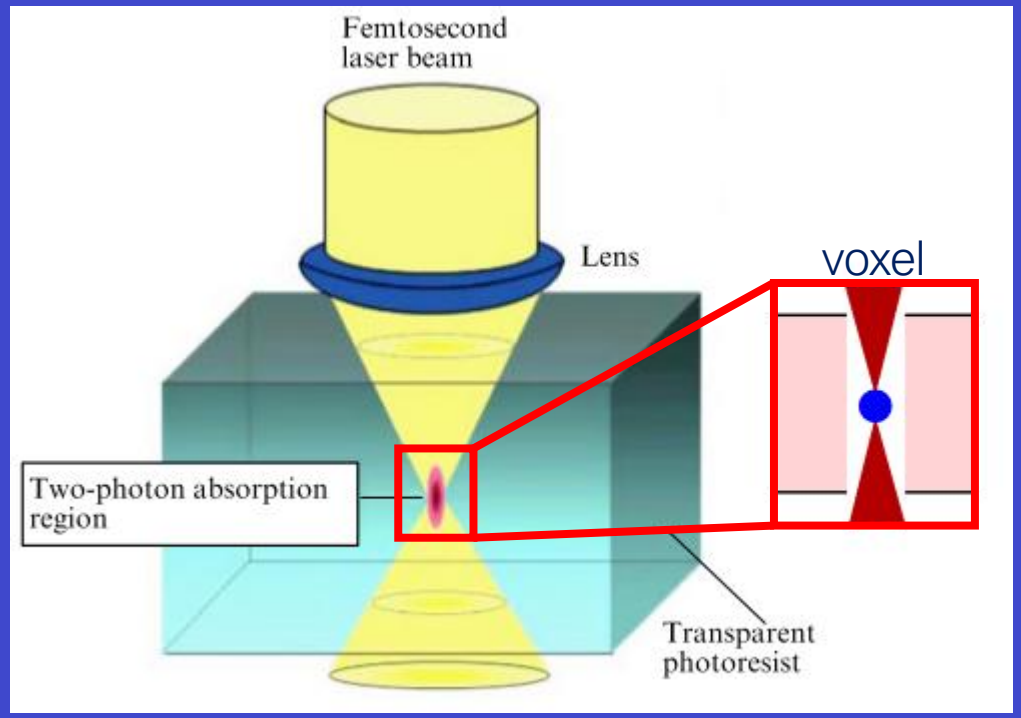

Voxel size is multivariable dependent, hence hard to control

(radiation power and wavelength, oxygen diffusion, the radiation dose, and the properties of photoinitiators and monomers)

In short, a highly sensitive and efficient photoinitiator and a low laser radiation wavelength result in smaller objects

Maruo S, Nakamura O, Kawata S Opt. Lett. 22 132 (1997)

Electrohydrodynamic inkjet printing

Sequential selective deposition of ink droplets onto a substrate, just like when printing a document.

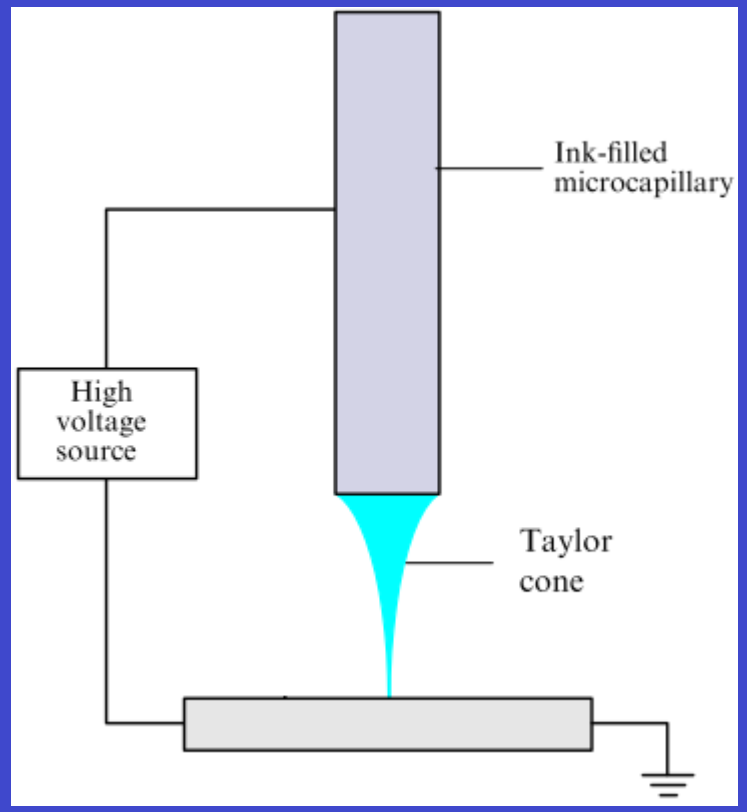

The jet diameter depends mainly on the electrodynamic force, rather than only on the ink viscosity as in conventional inkjet printing

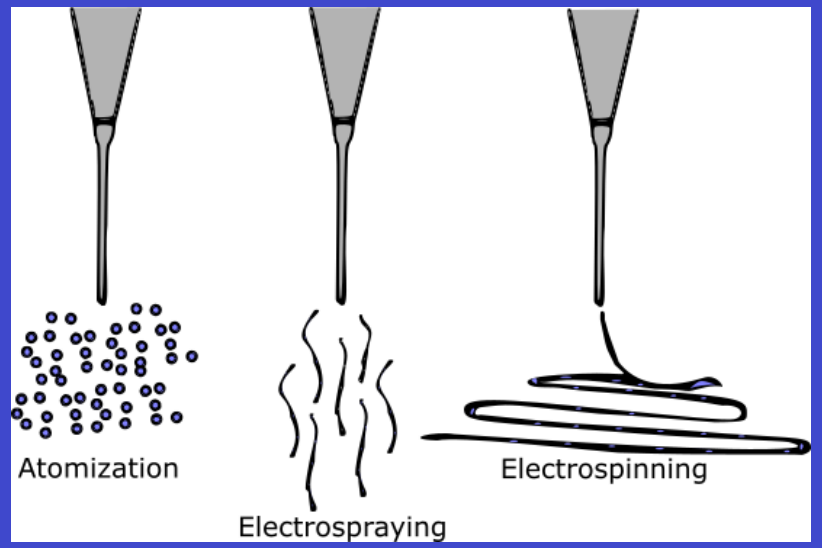

K.B. Fritzler, V.Y. Prinz, 3D printing methods for micro- and nanostructures, Uspekhi Fiz. Nauk. 189 (2019) 55–71. https://doi.org/10.3367/UFNr.2017.11.038239.

Laser-induced forward/backward transfer

The method is based on the transfer of a material from one substrate to another laser pulses.

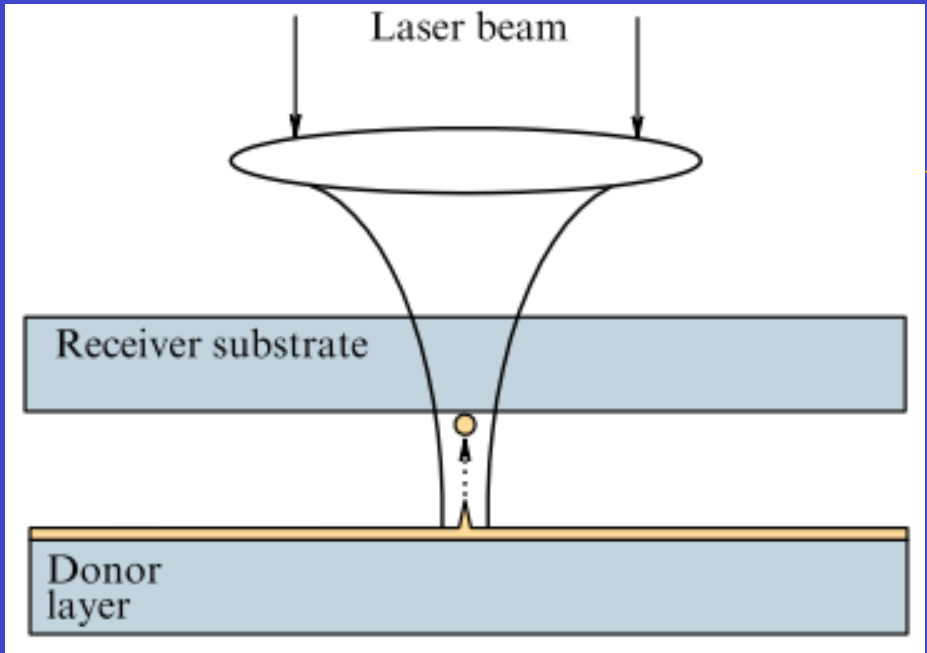

Laser-induced backward transfer

heating, melting, and subsequent crystallization

K.B. Fritzler, V.Y. Prinz, 3D printing methods for micro- and nanostructures, Uspekhi Fiz. Nauk. 189 (2019) 55–71. https://doi.org/10.3367/UFNr.2017.11.038239.

Conclusions:

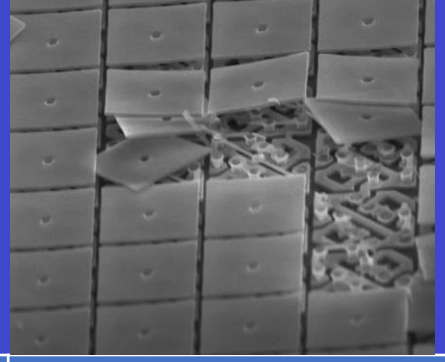

Scanning stereolithography	Projection stereolithography	Two-photon polymerization
Slow, but easy to maintain	Faster, but more sensitive	More versatile, but voxel is hard to control
Resolution is limited by the radiation wave-length		Higher resolution
Very slow processes –> rate of mm per sec		

EHD Inkjet printing	Laser-induced transfer
Fast process (cm per sec), can yield droplets and fibers	free from nozzle clogging, but the donor material may change
scalable, low cost, variety of materials	
The ink/donor properties alter the process	

How Digital Light Processing (DLP) works - YouTube, (n.d.). https://www.youtube.com/watch?v=9nb8mM3uEIc (accessed 20 May 2020).
V. Galstyan, M. Bhandari, V. Sberveglieri, G. Sberveglieri, E. Comini, Metal Oxide Nanostructures in Food Applications: Quality Control and Packaging, Chemosensors. 6 (2018) 16


Q&A

Physics – Uspekhi **62** (1) 54 – 69 (2019)

INSTRUMENTS AND METHODS OF INVESTIGATION PACS numbers: 32.80.Rm, 42.82.Cr, **61.46. – w**, **68.65. – k**, **81.20. – n**

3D printing methods for micro- and nanostructures

K B Fritzler, V Ya Prinz

DOI: https://doi.org/10.3367/UFNe.2017.11.038239

Contents

Abstract. The physical and physicochemical fundamentals of three-dimensional (3D) micro- and nanoprinting are presented. 3D printing (or additive manufacturing technology) is a process which fabricates structures and devices by depositing material (usually layer by layer) according to a 3D digital model. The methods and results reviewed here are limited to those from micro- and nanoscale fields, which are in demand in the fields of electronics, photonics, and bionics. Special attention is given to methods for fabricating sub-100-nm structures, including single- and two-photon polymerization stereolithography, electrohydrodynamic inkjet printing, and laser-induced forward transfer. The advantages and disadvantages of 3D printing methods are discussed, together with prospects for their development and application.

Keywords: 3D printing, additive technologies, 3D nanostructures, stereolithography, two-photon polymerization, inkjet printing, electrohydrodynamic printing, laser-induced forward transfer

1. Introduction

3D printing (or additive manufacturing technologies) is a process that forms structures and devices by depositing multiple layers of material according to a 3D digital model developed with the use of automated design systems [1]. The present review is focused on physical fundamentals of three-dimensional micro- and nanoprinting techniques, as well as their advantages and disadvantages. 3D printing is a rapidly evolving field of digital technologies, bringing radical changes to scientific, commercial, and industrial life. The review is confined to the methods and results allowing the production of micro- and nanoscale objects that are in high demand in electronics, photonics, bionics, and computer and information technologies. However, their application is limited primarily to manufacturing two-dimensional (2D) structures. Meanwhile, the necessity and inevitability of transitioning from planar micro- and nanostructures to functionally advantageous 3D ones have long been generally recognized [2–5].

3D printing provides a powerful tool for a revolutionary breakthrough in the fabrication of three-dimensional objects. It permits forming complicated structures that are impossible to obtain by other existing methods and techniques. Additive technologies have shown themselves to be highly adaptable, suitable for both large- and small-scale (even single-piece) production with high commercial efficiency [6–8]. 3D printing permits the use of a great variety of materials. Previous studies have demonstrated ample prospects for the use of 3D printing in the production of new micro- and nanodevices, structures, and materials in photonics (meta-materials, photonic crystals) [9], micro-optics (fiber end facet-coupled diffractive and focusing optical elements) [10], electronics (sensors, light-emitting diodes) [11], bioprinting [12–14], and bionics [15]. The scope of research and developments in the field of 3D printing based on new physical phenomena and effects (e.g., two-photon absorption, electrohydrodynamic phenomena, pyroelectric and photochromic effects, phase transitions, and holographic phenomena) are growing rapidly.

The format of the present paper does not allow comprehensively highlighting all aspects of 3D printing. It focuses on the most promising methods, such as laser stereolithography, laser-induced forward transfer of material, and electrohydro-

K B Fritzler, V Ya Prinz Rzhanov Institute of Semiconductor Physics, Siberian Branch of the Russian Academy of Sciences, prosp. Akademika Lavrent'eva 13, 630090 Novosibirsk, Russian Federation
Tel. +7 (383) 330 56 36. E-mail: kbf@isp.nsc.ru

Received 5 June 2017
Uspekhi Fizicheskikh Nauk **189** (1) 55 – 71 (2019)
DOI: https://doi.org/10.3367/UFNr.2017.11.038239
Translated by Yu V Morozov

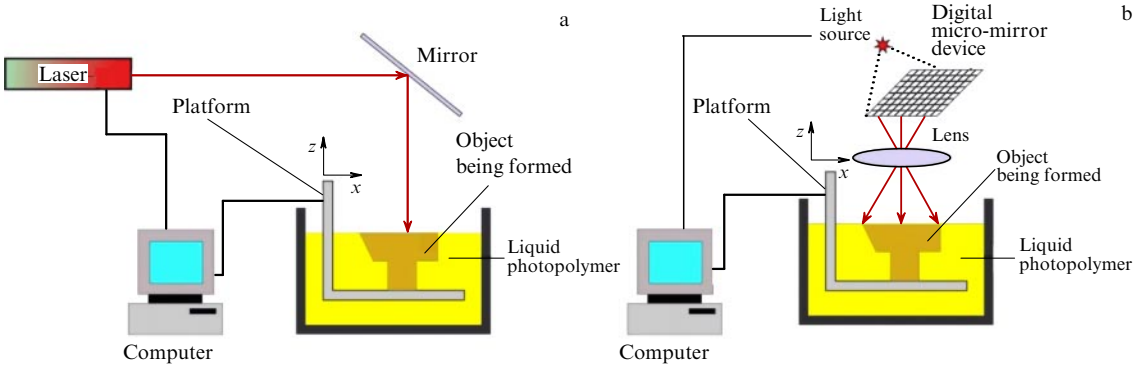

Figure 1. Layout of scanning (a) and projection (b) microstereolithography systems [21]. z is the platform movement coordinate.

dynamic inkjet 3D printing. Special attention is given to the advantages and disadvantages of 3D printing techniques, prospects for their further development, and applications.

2. Micro- and nanostereolithography

Stereolithography is one of the earliest and most popular additive manufacturing methods, patented by Charles Hull in 1986 [16]. It consists of layer-by-layer formation of 3D objects by photoirradiation of liquid photocurable materials [7, 16, 17]. Scanning and projection stereolithographic techniques are differentiated according to the light exposure regime [17]. In scanning laser stereolithography (SLS), a focused laser beam causes gradual point-by-point solidification (polymerization) of a photoresist in accordance with a digital model. Figure 1a shows an SLS system in which the platform on which an object is formed is placed in a bath with a liquid polymer to a depth equal to the single layer thickness (usually $\sim 10-100$ μm). As soon as the first layer is formed, the platform is submerged further to a depth equal to the thickness of the next layer, etc. The position of the laser beam on the photoresist surface is maintained by scanning the laser beam with the use of mirrors and precision horizontal movement of the platform.

The sequential character of scanning stereolithography markedly restricts its efficiency. Projection stereolithography in which the entire layer of a 3D object is simultaneously, illuminated, is free from this drawback. The principle of operation of a projection stereolithography apparatus is illustrated in Fig. 1b. An image of the 2D section of a three-dimensional computer model is projected onto the photopolymer surface by a digital micro-mirror device (DMD) [18–22] in the form of a silicon plate supporting a set of computer-controlled micro-mirrors. A DMD chip may contain several million $\sim 10 \times 10$-μm mirrors, each forming a pixel on the image. A mirror either projects the light flux onto the polymer or deflects it. The position of the mirrors is altered by electrostatic forces. Both projection and scanning stereolithographies make use of two main schemes of the process. Figure 1 shows photopolymer irradiation from above. It is equally possible to illuminate it through a transparent window in the bath. The object thus being formed grows upward successively to the height equaling the thickness of the illuminated layer.

A disadvantage of this method is its low resolving power, which usually does not exceed 10 μm. The natural desire to solve this problem accounts for a few interesting proposals that appreciably extend the applicability of the method.

2.1 Improvement in resolving power of stereolithographic methods

A drastic breakthrough in efforts to improve the resolution of stereolithographic techniques has been reached by developing the ability to manage the intricate set of physicochemical processes and events associated with photopolymerization [23]. Let us briefly consider them. Photosensitive initiator molecules introduced into a monomer solution undergo decomposition under the effect of optical radiation [24], giving rise to free radicals. Each molecule containing a radical binds a large number of monomeric fragments. In this way, the polymerization process is initiated, i.e., the formation of macromolecules from initially low-molecular weight monomers. The spatial distribution of radical concentration determines the minimal size of the object being formed.

Polymerization can be stopped by inhibitor molecules that interact with radicals and neutralize them. Oxygen is one of the powerful inhibitors penetrating into photoresists from the atmosphere or specially introduced into a starting solution [25, 26]. It will be shown below that the inhibitory activity of oxygen is employed in several methods to accelerate the printing process and improve spatial resolution.

The resolving power of optical methods is constrained by the Abbe diffraction limit [27]:

$$\Delta \sim \frac{\lambda}{2\mathrm{NA}},$$

where λ is the radiation wavelength and NA is the numerical aperture of the focusing system. However, taking advantage of the threshold character of the polymerization process permits the diffraction limit to be overcome. The spatial distribution of laser beam intensity in the focusing region is a Gaussian distribution. Therefore, the dose necessary for complete polymerization is reached only in the central high-intensity region of the laser beam, which can be below the diffraction limit.

3D objects measuring almost 1/100 the optical wavelength used for photopolymerization can be formed by a method based on two-photon absorption as proposed by Maruo in 1997 [28]. In this method, a laser beam transparent to the photoresist being used is focused onto a given point [28, 29] (Fig. 2a). Usually, the beam of a femtosecond laser (e.g., a Ti:sapphire one) with a ~ 810-nm wavelength is used to generate a pulse with a high peak power. In the central part of the focal spot, a threshold photon flux density

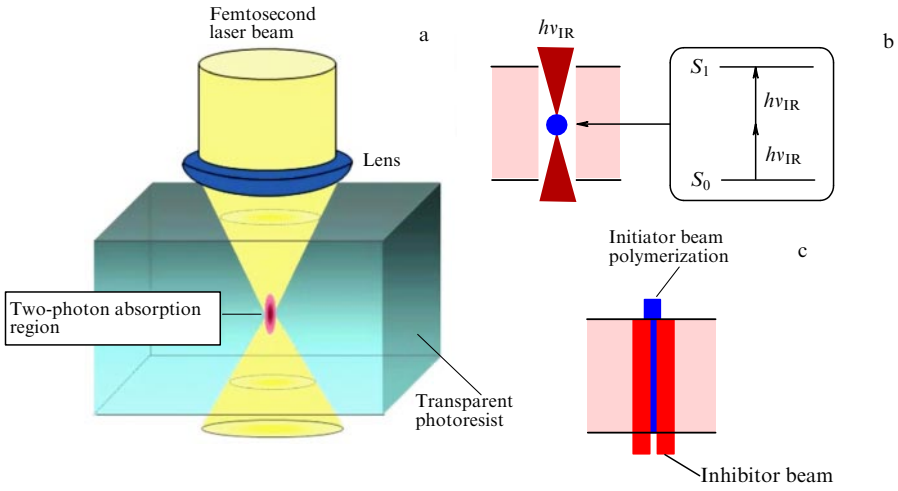

Figure 2. Two-photon polymerization processes [30]: (a) photoresist polymerization in two-photon absorption region; (b) schematic of two-photon transition between energy levels S_0 and S_1 of initiator molecule in two-photon absorption region; (c) relative position of initiator and inhibitor beams during stimulated emission depletion technique.

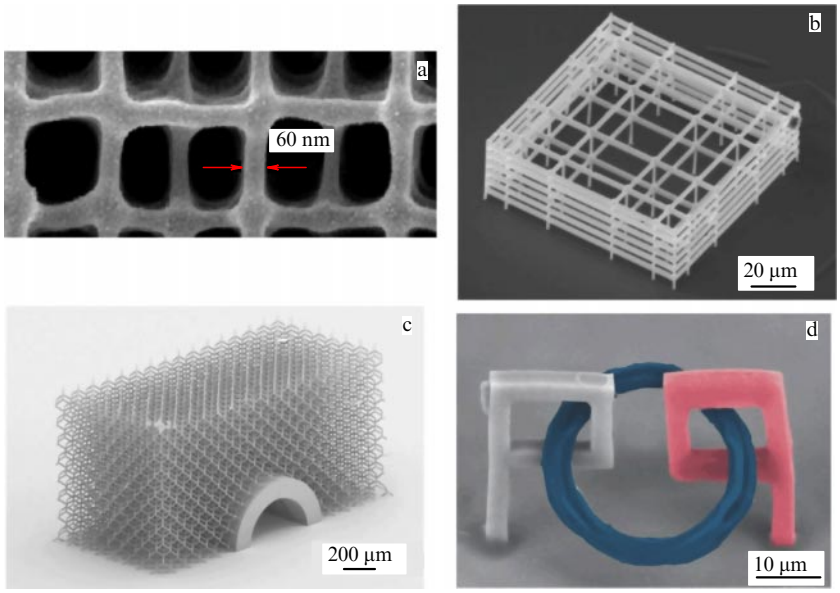

Figure 3. Examples of 3D structures formed by the two-photon polymerization technique (images obtained by scanning electron microscopy): (a) photonic crystal [41]; (b) scaffold [46]; (c) meta-material [36]; (d) intricately shaped 3D object: two microstructures from different materials joined together by a movable ring from a third material [47].

($\sim 10^{30}$ cm^{-2} s^{-1}) is reached, enough to trigger the two-photon absorption process initiating polymerization (Fig. 2b). The region of polymerization is called the voxel; it can be significantly smaller than the laser wavelength [30–33].

Both the voxel size and the resolution of the two-photon polymerization (TPP) method depend on a variety of factors, including those such as radiation power and wavelength, oxygen diffusion, the radiation dose, and the properties of photoinitiators and monomers [34, 35].

The very high resolving power and flexibility of the TPP method account for its wide applicability in micro- and nanophotonic, medicine, bionics, and many other fields. In addition, it is used to create meta-materials [36], photonic crystals [37–41], micro-optical elements [42–44], scaffolds for tissue engineering [45–47], and other 3D micro- and nano-structures. Figure 3 presents scanning electron microscopy (SEM) images showing 3D micro- and nanostructures obtained by the TPP method.

Of special interest is the possibility of developing micro-optical components integrated into optical fibers, light-emitting devices, and photonic chips (Fig. 4). Such integration is indispensable for processing and converting the light radiation being transmitted. Hybrid devices created by the TPP method can find application in fiber-optic communication lines and photonic microcircuits. The potential of the TPP technique was convincingly demonstrated by the formation of various optofiber micro-optical focusing and diffraction elements at the end of optical fiber [42, 44, 48–54].

The enhancement of the resolving power and capacity of the TPP method is the most serious challenge yet addressed through improvement in photoresist composition and characteristics of laser-based equipment. Specifically, the

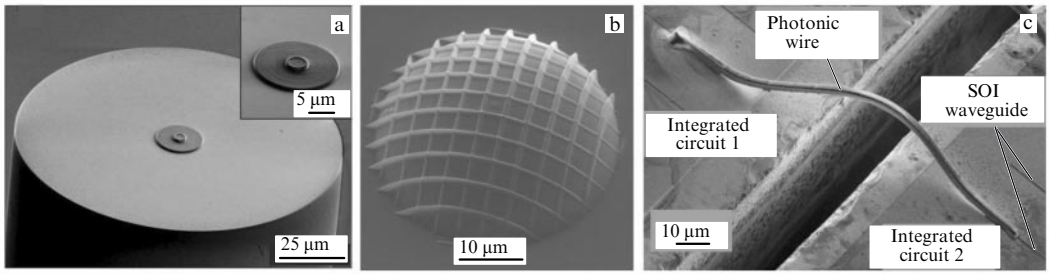

Figure 4. Microoptic elements formed by two-photon polymerization (SEM images). (a) Diffraction optical element formed at the optic fiber butt [52]. (b) Micro-lens with two-dimensional diffraction grating [54]. (c) Coupling of two photonic integrated circuits [53].

use of a highly sensitive and efficient photoinitiator allowed reaching a lateral resolution of 80 nm [55]. The lowering of the laser radiation wavelength to 532 nm made it possible to obtain photonic crystals with a minimal element size of 60 nm [41]. Theoretically, precision control of the exposure dose and polymerization threshold allows arbitrarily small objects to be fabricated. In practice, however, local irregularities in the photoresist, fluctuations in laser radiation intensity, and a variety of other factors limit the resolution [56, 57].

An elegant approach to decreasing the voxel size is provided by stimulated emission induced depletion (STED) technique based on the use of two lasers differing in wavelength. One of them (initiator beam in Fig. 2c) generates radicals and the other (inhibitor beam in Fig. 2c) prevents polymerization in the region of its maximum intensity [58–60]. Special focusing in the Gauss–Laguerre mode for the second beam ensures annular distribution of laser beam intensity. The peripheral part of the initiator beam irradiation region is characterized by maximum intensity of the inhibitor beam responsible for polymerization arrest [34, 59]. Such a system makes it possible to reduce the voxel size to 9 nm, i.e., to make it almost 1% the light wavelength (800 nm). To suppress radical generation, various physical mechanisms are employed [58, 61]. Details of this process are described in Ref. [59]. It should be noted that this method is too slow and complicated for wide application; moreover, it requires precise equipment and specific photoinitiators [62, 63].

A similar idea to use two lasers at a time is implemented in another method for obtaining polymer nanostructures with subwavelength resolution [64–68]. It is based on controlling the transparency of photochromic films and may find application in 3D printing. A photochromic coating is placed on top of the photoresist. A laser beam with the wavelength λ_1 and Gaussian intensity distribution makes this layer transparent and initiates polymerization by illuminating the photoresist (Fig. 5). In the region irradiated by the second laser with the wavelength λ_2, the photochromic layer becomes opaque. Beam intensity has an annular distribution, as in STED lithography, and reduces the region irradiated by the first laser. The proper initiator beam with the wavelength λ_1 triggers polymerization. This scheme makes it possible to form structures much smaller than the diffraction limit. By way of example, lines with an average width of 36 nm were obtained for a laser with $\lambda = 325$ nm [64].

Resolving power of the two-phonon polimerization technique can be improved using diffusion of inhibitor molecules at the low scanning speed of the laser beam [89]. Diffusion into the irradiation region makes up for the reduction in the inhibitor level during its interaction with

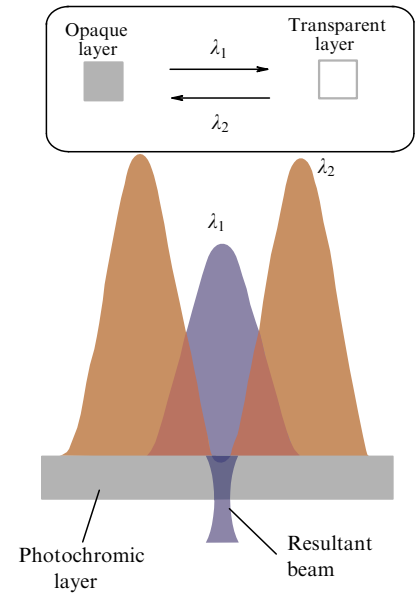

Figure 5. Two-beam scheme for the formation of nanostructures with subwavelength resolution based on photochromic layer transparency control (modified from [64]). A laser beam with wavelength λ_1 and Gaussian intensity distribution makes the photochromic coating transparent and triggers photopolymerization. The photochromic layer becomes opaque in the laser irradiation region with circular intensity distribution and wavelength λ_2. The resultant beam with wavelength λ_1 forms the polymerization region.

radicals. It enhances the radical production efficiency at the boundary of the voxel and further decreases its size.

The application of photopolymeric materials with nonlinear optical properties appears promising for the improvement of spatial resolution. Maruo in [70] proposed a method based on nonlinear single-photon polymerization. The nonlinearity is due to the presence of oxygen, an efficient inhibitor dissolved in the starting solution. As mentioned in a preceding paragraph, oxygen suppresses polymerization when interacting with radicals in the illuminated polymer volume. Polymerization can not be induced at low-intensity radiation, because all radicals generated by illumination are neutralized by oxygen molecules. In this case, as in TPP, the process has a threshold character but in the absence of two-photon absorption of light. Polymerization is initiated only in a local region of the focal spot where the necessary threshold radiation intensity is reached. This approach allows expensive femtosecond lasers to be substituted by lower-cost laser diodes without detriment to the spatial resolution of the formed structures. The potential of the method is demon-

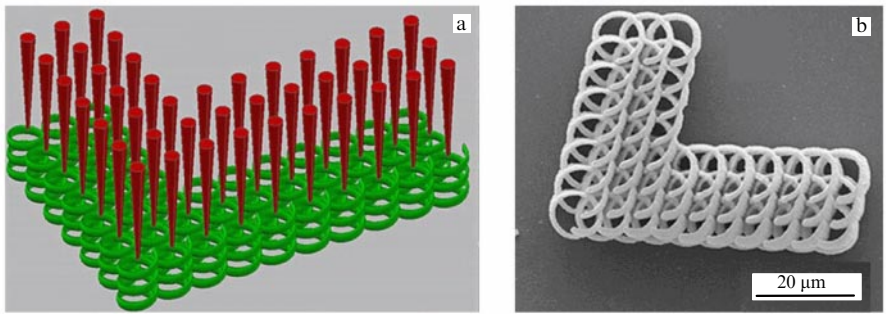

Figure 6. (a) Schematic formation of a helical photonic structure by multifocal two-photon polymerization. (b) SEM image of the final structure [89].

strated in [71], where the use of a continuous emission laser diode with a wavelength of 532 nm and a SU-8 photoresist allowed the forming of structures with a minimal size of 190 nm. To optimize single-photon polymerization, the underlying nonlinear physicochemical processes need to be better understood [25, 72–74].

2.2 Methods for increasing the performance of stereolithography

A low production rate is the main limiting factor precluding large-scale application of sequential additive technologies. For example, manufacturing a single 1 mm^3 photonic crystal takes over 10 days (at a beam scanning rate of 100 μm s^{-1} and line width of 65 nm [75]). Evidently, relevant technologies for TPP await optimization. Let us consider approaches to it.

One of them is the improvement of the scanning procedure for TPP. The formation of intricate structures requires precise synchronization of control over movements of the scanning system and the periodic turning on/off of the laser. This implies additional expenditures of time. The use of DMD together with a high-speed galvanometer scanner in the TPP method makes it possible to accelerate printing [76]. This technique was employed to obtain biomimetic structures with a minimal element size of up to 500 nm. The laser scanning rate can reach 3 cm s^{-1}. Scanning DMD by two laser beams [77] allows doubling the printing rate. Another obvious way to enhance the efficiency of laser micro-stereolithography is to increase the number of simultaneously illuminated points at which polymerization occurs and structures form. This approach is exemplified by technologies in which a laser beam splits into a few dozen or even hundreds of rays simultaneously illuminating the photopolymer [78–81].

Multiple focal points can be formed using diffraction optical elements [82, 83] or micro-lens arrays [79, 81, 84] having periodic spatial distribution. This allows parallel production of arrays containing only identical objects with a constant period, which makes the method insufficiently flexible for application.

Over recent years, an interesting and highly promising area has opened up due to the use of spatial light modulators (LMs) and computer-calculated holograms [85–88]. Structurally, a light modulator is a computer-controlled liquid crystal matrix. Diffraction of a laser beam on an LM is analogous to hologram reproduction and forms the necessary wave front. A computer calculates the holographic diffraction pattern for a given image that is used to set the optical properties of the LM. Alternation of calculated holograms downloaded onto the LM allows regulating the spatial distribution of laser radiation intensity and forming multiple focal points. Precision control of the intensity and position of each focus is possible with the use of computer-calculated holograms [89]. The number of resultant focal points is limited only by the power of the femtosecond laser. The method ensures independent control of intensity and movement of each focus, as well as its high positioning speed [90]. The high reproducibility of the process should also be mentioned.

Advantages of the method were demonstrated during the formation of micro-lens and photonic crystal arrays [89]. Seven micro-lenses 20 μm in diameter each were simultaneously (within 20 min instead of 320 min in the single-beam scheme) arranged to make up a hexagonal grid. Furthermore, 45 focal points were simultaneously used to form helical photonic structures (Fig. 6).

The speed of 3D printing can be further increased based on the above scheme with the use of computer software in combination with fast-operating galvanometric scanners [91] and arrays of micro-lenses [80].

Performance improvement is of primary importance not only for slow sequential methods but also for fast parallel additive technologies. In a traditional variant of projection stereolithography, UV radiation is used to illuminate the near-bottom layer of a cuvette. Then, the platform is elevated to make possible the renewal of the liquid polymer. In the end, the object being formed is placed back as far from the transparent bottom as the thickness of the new layer. Such sequential raising-and-lowering process takes time. The use of oxygen as the polymerization inhibitor made it possible to avoid these steps and turn the process into a continuous one [92]. To this effect, a so-called dead zone was formed between the bottom of cuvette and the object surface in the form of an oxygen-saturated fluid layer as thick as a few dozen micrometers (Fig. 7). This made possible the continuous renewal of the liquid polymer layer near the object edge and allowed continuity of the polymerization process to be maintained. The method, called 'continuous liquid interface production of 3D objects' by the authors, enhanced the efficiency of projection stereolithography by almost a factor of 100 [92].

3. Inkjet 3D printing

Inkjet printing (IJP) has been developing as a technology for image formation with the use of microscopic ink droplets deposited onto paper or textiles for centuries. The first electronic devices using this technique and designed to create two-dimensional images on paper appeared in the 1950s. Thereafter, the method developed in different directions and has found application in additive manufacturing since the 1980s. In this technique, 3D structures are formed according to a computer model by sequential selective deposition of ink droplets onto a substrate [7, 93]. IJP is widely employed in

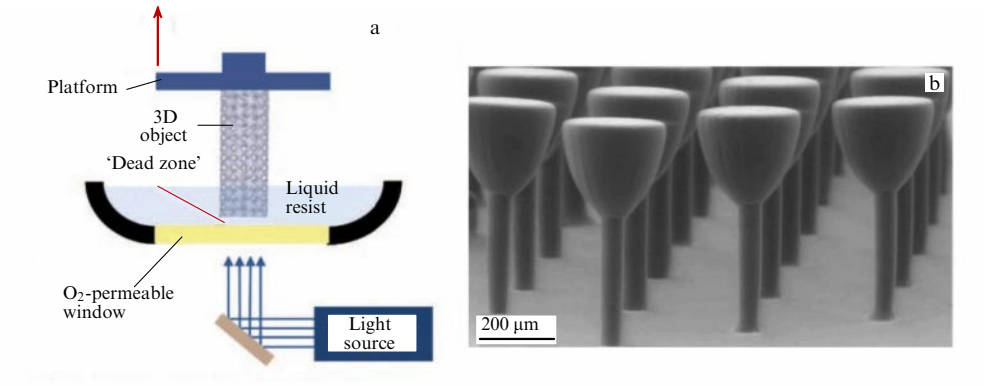

Figure 7. Technology of continuous liquid-interface production. (a) Schematic and (b) specimen of the formed structure (SEM image) [92].

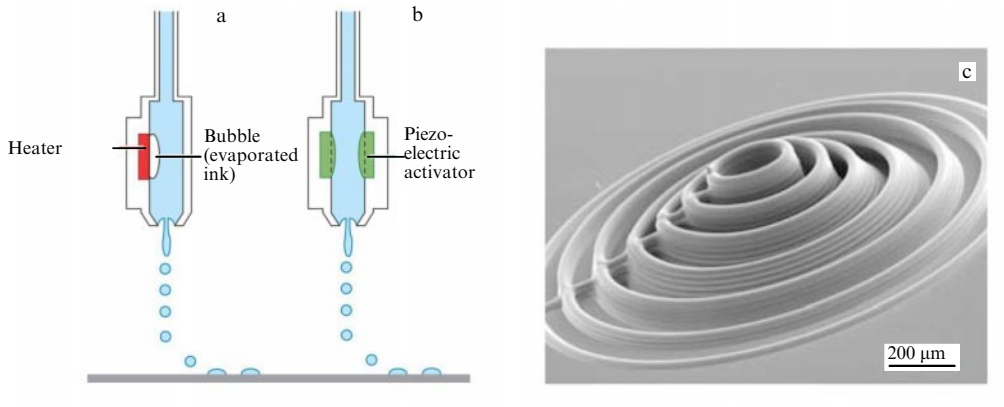

Figure 8. Inkjet printing: (a) thermal, (b) piezoelectric [93]. (c) SEM image of printed silver micro-electrode [116].

organic and hybrid electronics. It provided a basis for printed electronics in which macro- and nanolayers of functional inks differing in electronic properties are sequentially printed on a flexible substrate [94]. This section focuses on the physical principles behind different IJP techniques used to manufacture micro- and nanostructures, tools, and materials.

Inkjet 3D printing makes use of a great variety of materials to form 3D structures. Such materials are referred to as ink. They include colloid solutions of nanoparticles, polymers, metals, composites, glasses, and biological tissues. A wide spectrum of materials [95–99] and the possibility for successive transitions from one material to another provide a basis for producing many-layer heterostructures with different functional (optical, electronic, and biological) properties.

To recall, IJP techniques differ in ink jetting regimes and are categorized into continuous inkjet technology and drop-on-demand inkjet printing [100]. The latter method is more frequently used in additive manufacturing [96].

Figure 8 illustrates the operating principle of an IJP device. The activator built into a capillary with liquid ink exerts either thermal or piezoelectric action on it, which ejects a droplet through the nozzle onto the substrate. In thermal printing, a printhead mounted above the nozzle contains thermoelements receiving current pulses that heat them and thereby the ink, which undergoes local evaporation accompanied by air bubble formation (Fig. 8a). The bubbles increase in volume and expel ink droplets through the nozzle onto the substrate at a pressure in excess of 125 atm. The operational efficiency of the system is 160,000 droplets per second [101]. In piezoelectric printing, a piezocrystal placed over the nozzle undergoes deformation under the effect of electric current, which makes an ink droplet pass onto paper (Fig. 8b).

3.1 Parameters determining the quality of inkjet printing process

High-quality printing requires both understanding and fine tuning the processes involved in the formation, movement, and interaction of ink droplets with the substrate material. Let us consider the main parameters influencing the quality of inkjet printing. Both the shape and the length of the control pulse have as great an influence on the reproducibility of the printing process as they have on the droplet size, stability, and velocity [102].

Surface tension, inertia, and viscosity play key roles in the formation and behavior of a droplet and fluid stream. Ink viscosity must be low enough to enable its unobstructed movement in printhead capillaries and surface tension sufficiently high to avoid uncontrolled fluid leakage from the nozzle. Hard particles present in the solution tend to clog the capillaries, which is of special relevance for high-resolution 3D printing with maximum resolution where capillaries up to 1 μm in diameter are used [101].

Surface tension transforms the ink flow ejected from the nozzle into a spherical droplet. In the case of an inadequately chosen control impulse, the flow can split into several droplets, which should be avoided in 3D printing because it compromises the resolution of the method [103].

Collectively, the generation of a droplet and its transport to the substrate make up a complicated process depending on a variety of factors. It is characterized by dimensionless

quantities, such as Reynolds, Weber, and Ohnesorge numbers [104, 105] describing the relationships among droplet diameter, speed, inertial forces, viscosity, and surface tension. An analysis of mechanisms behind droplet generation has yielded stability criteria for 3D printing [93].

Of primary importance is the droplet-substrate interaction, as well as ink-drying and post-printing processes. Too high a speed of a droplet hitting the substrate may result in droplet deformation and breakup into a few small droplets. Ink drying is likely to produce the so-called 'coffee stain' effect, having an important influence on the morphology of the resultant structures. It is caused by the nonuniform distribution of the drying material that migrates from the center to the edge of the droplet where its thickness is much greater. This phenomenon is attributable to the nonuniform evaporation of the fluid over the droplet surface [106]: it is higher near the fixed boundary of the droplet, which gives rise to convective streams, tending to compensate for fluid loss, and increases the concentration of the dissolved material at the periphery [103, 107–110]. It is possible to avoid this effect by shaping a centripetal flow, making up for the convective stream due to the coffee stain effect. Binary solutions containing components with different boiling points [111–113] or surfactants [114] are used for the purpose.

The minimal size of the structures formed using IJP depends on the droplet size and is limited by the nozzle diameter. In most cases, it is below 10 μm [37], but sometimes can be much smaller [115].

Creating 3D objects by the IJP technique implies the necessity of a combined approach to the control and improvement of all parameters of the process. In 3D printing, the material is deposited not only on a prepared substrate as in 2D printing but also onto the previously formed layers, provided that each of them has optimal characteristics for printing the next layer and resists deformation from subsequent deposition. It imposes additional requirements on the surface of the layers being formed, ink properties, and parameters of the printing process. Numerous efforts to address this problem have yielded a variety of approaches to obtaining 3D structures by IJP. Let us consider some of them.

Controlling ink rheologic properties allowed 3D metal structures to be shaped with a high aspect ratio (length to width) using nozzles 1 μm or more in diameter and inks containing a 71% solution of 5-nm silver nanoparticles. Sequential layer-by-layer deposition yielded conducting structures with a minimum diameter of 2 μm [116] (Fig. 8c).

To control the physical properties of the substrate, it can be coated with hydrophobic or hydrophilic materials. This approach is used to improve the resolution of the self-aligned printing technique for manufacturing thin-film transistors [117, 118]. First, a drop of a conducting composition is placed on the substrate to form a contact. Then, the substrate is treated in a plasma and covered with a special surface active agent to form the hydrophobic coating. Thereafter, a second drop is printed, which rolls down the hydrophobic surface; after it dries out, a 60–400 nm gap appears between the electrodes.

Another approach includes the use of ink containing a fast-evaporating solvent. In this case, the solvent present in the deposited droplet evaporates before the next layer is placed. In this way, structures (nanocolumns) with an aspect ratio of 50:1 and a minimal diameter of up to 50 μm were obtained [119]. A low-viscosity ink (< 0.554 mPa s) was used

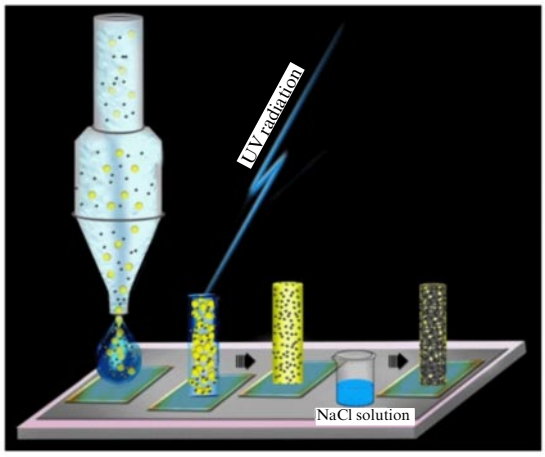

Figure 9. Inkjet 3D printing of a conductive structure. The ink used is a UV-curable photopolymer containing silver nanoparticles [120]. Post-printing treatment of the material in an NaCl solution and sintering improves its conductive properties.

(a 30% colloidal solution of 2–4-nm gold nanoparticles in toluene). The nozzle diameter was 50 μm, the solvent evaporation time ~ 380 ms. The size of the resultant objects could be reduced by heating or *in situ* laser annealing of the substrate during printing.

Special photopolymers find application in both inkjet printing and stereolithography. Printing each layer using a polymer ink is followed by its UV curing [120] (Fig. 9]. The addition of metal, fluorographene, or graphene nanoparticles to a photopolymer [121] makes it possible to obtain conducting or insulating 3D structures to serve as contacts, conductors, and insulators in printed electronics.

Post-treatment processes play a key role in inkjet printing. As a rule, deposition of a material is followed by drying or annealing for the shaping of a functional layer with predefined features. For example, printing with metal inks requires heating to 100–300 °C to improve the electrically-conductive properties of the printed objects with the use of microwave [122, 123], laser [124], optical [125], electric [126], and plasma [127] heating options or their combinations [123]. Studies aimed at developing inks that do not need thermal treatment after printing are underway [128]. Colloidal solutions of metallic nanocrystals coated with the conducting polymer poly[2-(3-thienyl)-ethyloxy-4-butylsulfonate] (PTEBS) have been proposed [129]. The use of this material ensures high electric conductivity of printed layers in the absence of a post-printing thermal treatment.

3.2 3D nanostructure inkjet printing

One of the main current trends in the development of IJP techniques is the reduction of droplet volume during printing. The most obvious way to this goal is to decrease the nozzle diameter, but it is fraught with the problem of clogging by particles suspended in the ink. Marked progress was reached by the use of an electric field for diminishing the droplet size as in electrohydrodynamic (EHD) inkjet printing [130–133]. An electric voltage is applied between the nozzle of the printhead and the substrate (Fig. 10). The fluid in the droplet is charged either positively or negatively, depending on polarity. The charges accumulate at the top of the droplet as the applied voltage grows. Finally, Coulomb repulsion forces between ions and the electrostatic attrac-

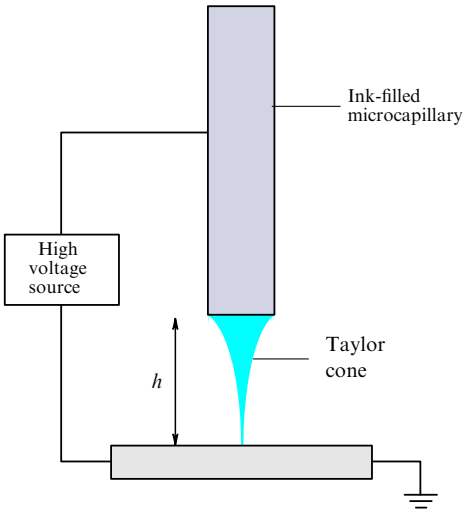

Figure 10. Schematic of electrodynamic inkjet printing setup [133].

tion to the substrate cause a deformation of the semispherical meniscus, which takes a conical shape referred to as a Taylor cone [134]. At a certain critical electric field, a thin stream of the fluid leaves the droplet surface. The droplets or jets thus formed have a diameter several times smaller than the nozzle diameter. By varying the conditions of the process (field characteristics, viscosity, and speed of the fluid flow), it is possible to deposit a continuous ink stream (electrospinning [135]) or separate droplets (drop-on-demand inkjet printing) onto the substrate [136]. The possibility of shaping three-dimensional microobjects (heterostructures) from several materials by electrodynamic printing has been demonstrated [137].

The EHD printing technique combines high resolution and the possibility of simultaneously using several materials for manufacturing 3D structures. The synergistic effect of these advantages is shown in Ref. [138], where high-resolution (250 nm) color pictures were obtained. Droplets of three different colloidal solutions of quantum dots giving three process colors (red, blue, and green) were placed on the substrate (Figs 11a, b). Pixels of various hues were formed by sequential deposition of solutions containing quantum dots emitting primary colors. The droplets were $\sim$ 100 nm in size. This technology opens up good prospects for manufacturing transparent electrodes for sensor screens, quantum dot-based light sources, and plasmon nanostructures.

The EHD printing method provided a basis for the development of metallic 3D nanostructures [139, 140]. Ink nanodroplets containing metal particles were sequentially generated on a Taylor cone, were accelerated in an electric field, and reached the substrate, where they rapidly evaporated, giving rise to the next layer with uniformly distributed metal particles. The top of the growing nanocolumn functioned as a pointed electrode, creating a strong electric field gradient. This promoted additional 'focusing' of falling charged droplets and the maintenance of a constant diameter of the growing structure. This method was employed to shape gold nanocolumns up to 50 nm in diameter with an aspect ratio of $\sim$ 17 [139]. A nozzle with a diameter of 600 nm was used. The ink was a 0.1-vol.%. gold nanoparticle solution in n-tetradecane. Also obtained were grids of metal electrodes from 80 to 500 nm in width with an aspect ratio of up to 3 (Figs 11c, d) [140].

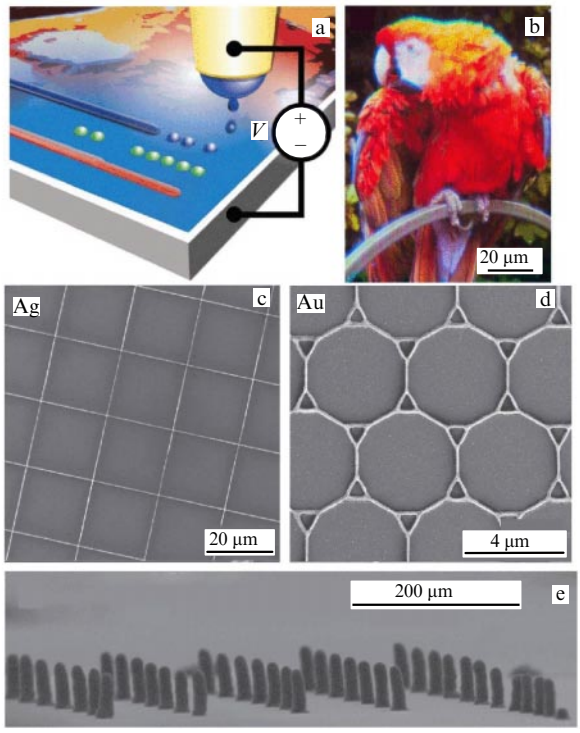

Figure 11. (a, b) High-resolution EHD printing of color pictures with the use of colloid quantum dots [138]: (a) the device, (b) 94 × 125-μm color picture of a parrot, (c, d) SEM images of different 3D structures obtained by the EHD printing technique [140]: (c) square silver electrode grid with 20-μm spacing and aspect ratio 2.5, (d) $\sim$ 80-nm-wide hexagonal gold electrode grid with aspect ratio 2.3. (e) Array of 100-μm-high microcolumns 12 μm in diameter with aspect ratio of $\sim$ 8 formed by the EHD printing technique from molten wax [141].

As mentioned above, polymer and wax melts are used for EHD printing. These materials are maintained in the liquid state by heating in a microcapillary. The ink solidifies immediately after deposition onto the substrate. This method was used to obtain 3D structures with a minimal size of 10 μm and aspect ratio of $\sim$ 8 (Fig. 11e) [141].

The problem of performance enhancement is equally relevant for inkjet printing and stereolithography. It is partly solved by increasing the number of nozzles in printing heads [142–144]. One of the approaches to parallelization of the method is the production of microcapillary matrices playing the role of nozzle orifices for electrohydrodynamic 3D printing, which are formed by the photolithographic technique [145, 146].

The authors of [147–149] proposed to simplify 3D printing by making use of the pyroelectric effect in lithium niobate (LN, a material capable of spontaneous polarization). In equilibrium, the electric field conditioned by spontaneous polarization is completely screened by free charges on the crystal surface.

A rapid local change in crystal temperature by ΔT alters polarization and results in the appearance of the uncompensated charge $\sigma = p\Delta T$ (p is the pyroelectric constant) on the surface. Quantity p for LN is 4×10^{-5} C m^{-2} K^{-1}, which gives an electric field strength of $\sim$ 10 kV cm^{-1} upon crystal heating by 100 °C. Such strength corresponds to the values used in EHD printing and initiates analogous processes. Specifically, ink drops undergo deformation, giving rise to a Taylor cone; then, the fluid is discharged toward the substrate

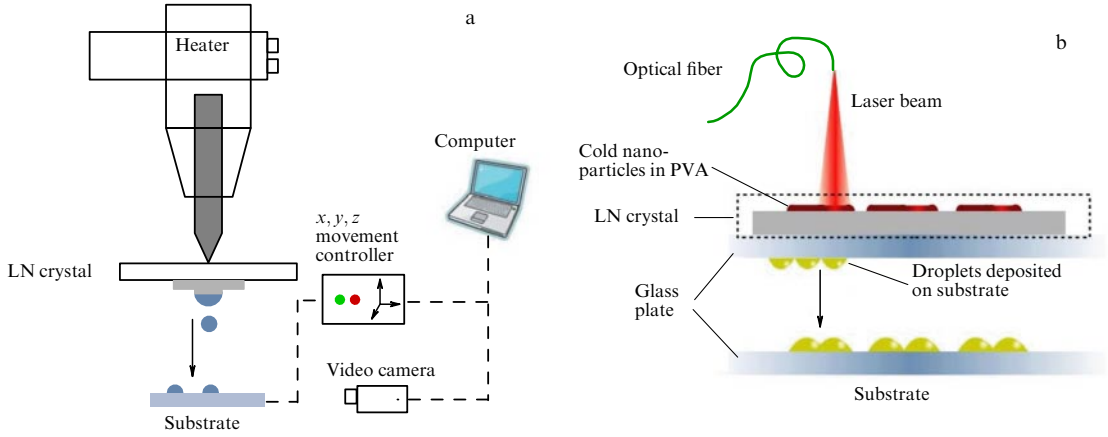

Figure 12. (a) Schematic of pyroelectric EHD jet printing machine. An electric field is generated by local heating of lithium niobate (LN) plates. (b) The use of plasmon resonance to improve resolving power of pyro-EHD printing. Plasmon resonance is excited in gold nanoparticles by laser radiation (810 nm) [150].

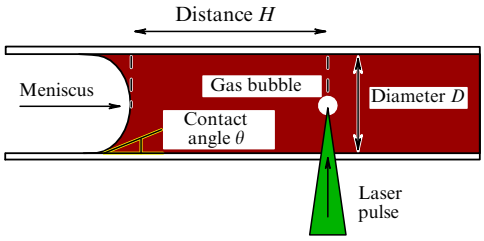

Figure 13. Microdroplet generation by a laser pulse. The diagram shows parameters influencing droplet size: distance from laser focal point to meniscus H; contact angle between meniscus and capillary surface θ; capillary diameter D [151].

(Fig. 12a). Point heating of the lithium niobate plate is performed by either a hot probe or an IR-laser. The minimum diameter of the droplet obtained by this method is 600 nm [148].

The spatial resolution of pyroelectric printing can be improved by the deposition of gold nanorods onto the lithium niobate plates [150]. Laser radiation with a wavelength of 810 nm excites localized plasmon resonance in these nanoparticles (Fig. 12b), causing heating of Au particles and a local rise in LN substrate temperature. In this way, the pyroelectric effect generates an electric field.

One more method for reducing the droplet size in inkjet printing makes use of hydrodynamic impact. It was proposed to initiate droplet generation by a nanosecond laser pulse focused near the meniscus in the capillary [151, 152] that forms a gas bubble in the fluid volume (Fig. 13). The compression wave generated in this process acts like a hydrodynamic shock on the concave ink surface in the capillary and produces a focused micro-jet with a speed higher than the velocity of sound. The resulting droplet can be one tenth the inner capillary diameter [152].

The inkjet printing technique provided a basis for the development of an additive technology allowing 3D structures of any desired shape to be made from nanofibers [153, 154]. A micropipette containing a polymer solution (a 1.3–2.6% aqueous PEDOT/PSS solution) is brought into contact with the substrate. The monomer solution forms a meniscus at its end (Fig. 14). As the pipette tip is drawn upwards, the meniscus becomes elongated and thinned, making up a nanofiber. After its size decreases to hundreds of nanometers, it undergoes polymerization due to the interaction with oxygen in the air. Varying the stretching rate permits regulating the size of the nanofiber and obtaining structures measuring from a few micrometers to 100 nm.

Today, inkjet printing is the fastest growing printing technology, finding application in various sectors of science and industry. IJP methods have been used to manufacture solar cells [155], photodetectors [156], transistors [157], light-emitting diodes [11], memory elements [158], and micro-lenses [144, 159, 160]. Some of these devices have characteristics highly competitive with those of the best specimens obtained by standard methods [161].

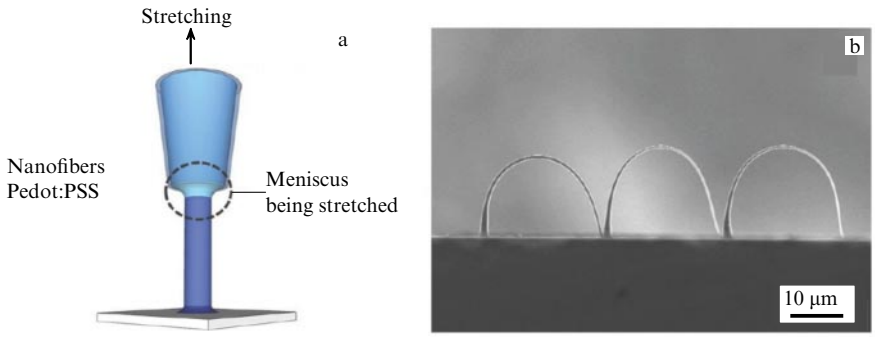

Figure 14. (a) Schematic of 3D structure formation from nanofibers by inkjet 3D printing [153]; (b) SEM image of a set of nanoarches formed from nanofibers with a radius of 200 nm.

The use of 3D printing methods is a highly promising approach to the integration of electronic structures into biomaterials. Developments in this area are exemplified by the bionic ear [15], i.e., a computer model of the human ear created using computer-aided design (CAD) software. The IJP technique was employed to print, in accordance with this model, a hydrogel matrix with polymeric channels containing silver nanoparticles and making up a spiral antenna. Then, auricular cells were placed into the hydrogel matrix. This work demonstrated the possibility of 3D printing of biologically and electronically functional tissues.

The following advantages of IJP account for the great interest in this method:

• Technical simplicity and low cost. No expensive vacuum technologies are needed. A marked reduction in production costs is achieved by shortening the technological chain, eliminating necessity for mask making, and saving materials by means of additive manufacturing.

• The possibility of working with virtually any sort of substrate or material. The low-temperature technological process allows a wide spectrum of flexible substrates to be used.

• Environmental friendliness. The method is more environmentally compatible than subtractive technologies, since it does not require the removal of the deposited material with the use of large amounts of toxic chemical reactants.

• Universality and flexibility. A single jet printer can be used to produce a variety of devices, such as light-emitting diodes, solar cells, transistors, and photodetectors, by slightly changing the parameters of the CAD model and functional inks.

• The possibility of scaling. IJP allows the creation of devices of various surface areas, from 1 μm^2 to 1 m^2.

• Compatibility with high-performance roll-to-roll processing [162], where structures are shaped by continuously feeding a flexible substrate from a roll and depositing functional ink, followed by relevant technological operations. This approach ensures a high production rate, which makes it attractive for large-scale manufacturing [163].

• Simplified transfer of technology, entailing the disclosure of ink formulation and a file containing a 3D digital model. This opens up good prospects for information exchange among laboratories and between developers and manufacturers. Such an approach is impossible in traditional production methods and represents a new paradigm for both basic research and applications.

4. Laser-induced forward transfer of material

The laser-induced forward transfer (LIFT) of material is an efficient method using laser radiation for additive deposition of materials.

The method is based on the transfer of a material from one substrate (donor) to another (acceptor) under the effect of a laser pulse. The sequential transfer allows shaping, layer by layer, 3D structures [164–166] from metals [164, 166–168], inks [169–171], or pastes [172] deposited onto a transparent substrate. The transfer is initiated by a laser beam that passes through the transparent substrate and is absorbed by a donor material that undergoes local heating (Fig. 15a). This causes melting and evaporation of the donor material in a localized region bordering the carrier. The melting front rapidly propagates toward the film surface. Vapor pressure between the melt and the substrate generates the motive force driving the melted material to the receiver substrate [164, 173]. The minimum size of the element transferred by the LIFT method is 70 nm [174].

One of its advantages is the possibility of working with a great variety of materials, including metals, organic matter, and nanoparticles in any form (as solids, ink, or paste). The diameter of droplets transferred onto the substrate can be much smaller than that of the laser focal spot. For example, droplets 330 nm in diameter were obtained with the use of a femtosecond Ti:sapphire laser producing a light spot 4 μm in diameter on the donor substrate coated with a 30-nm-thick Cr layer [167].

The LIFT process, similar to IJP, is compatible with high-performance roll-to-roll processing and can be introduced in efficient large-scale production [175, 176]. At the same time, this method is free from nozzle clogging problems inherent in inkjet printing technologies.

Electrical and structural characteristics of deposited materials can change during heating, melting, and subsequent crystallization, which leads to deterioration of the functional properties of the final structures. A number of modifications have been proposed to address this problem and extend the potential of the approach. One of them is the dynamically separable layer method, based on the use of a special layer between the substrate and the donor film that absorbs radiation [177]. Both metal (Au, Ti) and polymer films are used for the purpose [178–181]. The interaction of the laser beam with this layer causes ablation of the buffer layer in the beam focal region and discharge of the donor material (Fig. 15b).

There is a method in which the transfer is initiated by bubbles from the evaporated material [182, 183]. A polymer layer a few micrometers thick absorbing laser radiation lies between the transparent substrate and the ink donor layer. Laser radiation partly evaporates the polymer, giving rise to a rapidly expanding bubble that directs the ink jet to the acceptor substrate (Fig. 15c). The remaining polymer layer serves as a buffer protecting the ink from thermal and mechanical impacts.

In another method, known as laser-induced backward transfer (LIBT), the transparent acceptor substrate is placed over the donor substrate (Fig. 15d) [184]. The laser pulse is focused through the receiver substrate onto the donor layer (metal, polymer, or silicon), where it is absorbed and causes local melting accompanied by metal expansion and a rise in pressure. Strong temperature and pressure gradients, together with surface tension, force form in the melted metal a stream with a droplet at the top moving toward the receiver substrate [185]. The droplet diameter can be modified by varying the donor film thickness, pulse energy, and focusing. LIBT with a 10-nm-thick gold film allowed obtaining droplets 220 nm in diameter using a femtosecond laser with a wavelength of 800 nm and a pulse energy of 0.9 mJ. The substrate to substrate distance was less than 10 μm.

In LIBT, as in LIFT, the functional properties of donor materials are protected by special buffer layers [186]. A silicon plate can be used as the donor substrate [187] The liquid silicon density, unlike that of metals, is higher than in the solid state. In the case of a Gaussian spatial distribution of laser beam intensity, the molten volume decreases and forms a toroidal ring at the periphery of the irradiated region. Such a shape and liquid silicon dynamics are attributable to the temperature dependence of surface tension. The maximally heated melt in the center of the focal spot has minimal surface

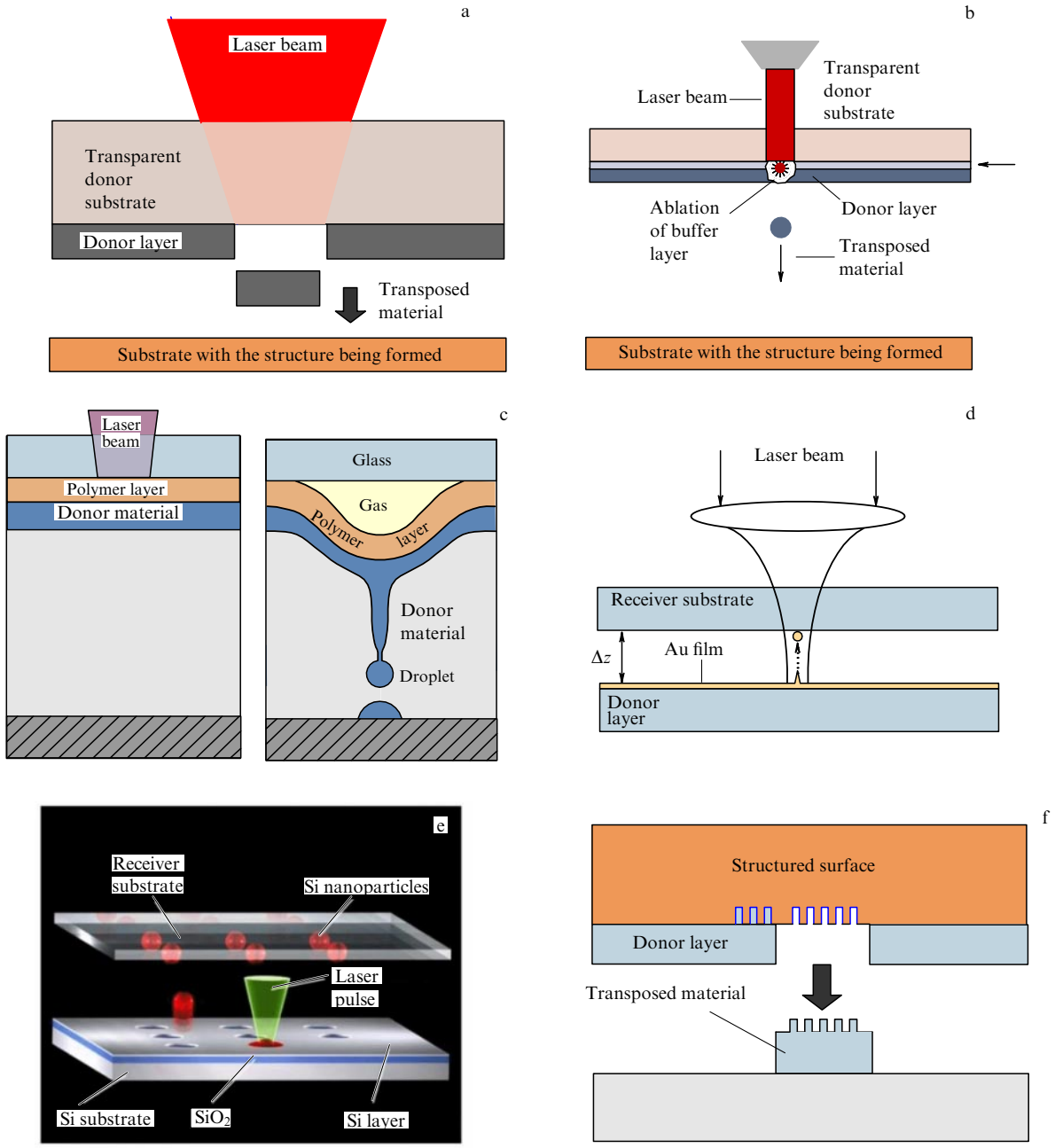

Figure 15. Variants of laser-induced forward transfer. (a) General diagram of the method [179]. (b) Dynamically separable layer method. Laser radiation is absorbed in a buffer layer, which leads to its local ablation and therefore discharge of donor material. (c) Transfer by gas bubbles resulting from evaporation of the buffer polymer layer [182]. (d) Laser-induced backward transfer [184]. (e) Laser-induced backward transfer with the use of a silicon-on-insulator structure as the donor substrate [188]. (f) Laser-induced transfer of material with a structured surface; a relief is formed on the donor substrate before depositing the donor layer by nanoimprint lithography [189].

tension, responsible for the movement of liquid silicon toward a colder region. The molten zone is unstable, and surface tension forces cause a few droplets to be ejected toward the acceptor substrate. If a laser beam with an annular intensity distribution is used, the minimal temperature region lies in the middle of the focal spot whither the liquid silicon flow is directed. In this case, controlled discharge of a droplet toward the receiver substrate is possible. The use of silicon-on-insulator as the donor substrate permits the size of the nanoparticles produced to be reduced to 160 nm [188]. This process is schematically presented in Fig. 15e.

Figure 15f illustrates the creation of a nanorelief on the donor substrate surface by imprint-lithography. This method can be used to produce objects up to 5 μm in size with a structured surface from ~ 140-nm elements [189]. Integration of 3D printing and subtractive technologies provided new interesting approaches, as exemplified by the hybrid methods overviewed in Section 6.

Similar to stereolithographic techniques, LIFT makes use of digital micro-mirror devices and spatial light modulators [190–192]. Some structures obtained by LIFT are shown in Fig. 16.

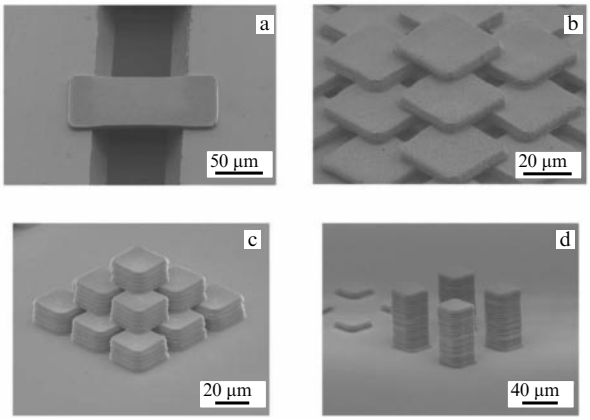

Figure 16. SEM image of microstructure formed by laser-induced forward transfer [165]. (a) A bridge on a 100-μm-wide Si-channel; (b) scaffold; (c) micro-pyramid; (d) micro-columns.

5. Subnanometer resolution methods

The above additive techniques make it possible to form structures hundreds and even tens of nanometers in size. Today, developers of additive technologies are faced with a more ambitious task: using single atoms as building blocks to shape 3D structures. The achievement of this goal would open up unparalleled opportunities for designing novel heteromaterials and devices. The problem is addressed with the use of the tools that have already shown themselves to be advantageous in nanotechnologies but are most frequently employed in subtractive processes or for shaping 2D objects. They include electron and ion beams, cantilevers of atomic force microscopes (AFM), and carbon nanotubes. Attempts to develop additive techniques based on these tools for manufacturing 3D structures with maximum resolution have resulted in the improvement of existing methods and the appearance of new ones.

High spatial resolution is attainable by gas-phase deposition in a chamber with a precursor gas. The local impact of a laser, electron or ion beam on precursor molecules adsorbed on a substrate results in reactant decomposition and deposition of the material onto the substrate (Fig. 17a). Beam scanning of the substrate surface in accordance with a given program allows forming, in the layer by layer manner, three-dimensional structures [193–201]. Gas-phase deposition initiated by electron or ion beams ensures a spatial resolution of up to 50 nm (Figs 17b, c), but the structure growth rate remains rather low (10–50 μm s^{-1}) [202]. The laser beam causes the most efficient deposition. As was mentioned above, the laser beam scanning rate may be as high as a few millimeters per second, but the spatial resolution does not exceed 1 μm [7, 202].

An interesting method was described in [193], where multi-walled carbon nanotubes were used as emitters in electron beam-induced gas-phase deposition systems. Deposition was performed onto an Au film-coated silicon substrate used as an anode. The emitter consisted of carbon nanotubes placed on an AFM cantilever 377 nm from the substrate. The authors obtained structures with lateral and vertical resolutions of up to 200 and 70 nm, respectively. It was proposed to use arrays of carbon nanotubes to pass to the parallel structure formation process and enhance the performance of the method [193].

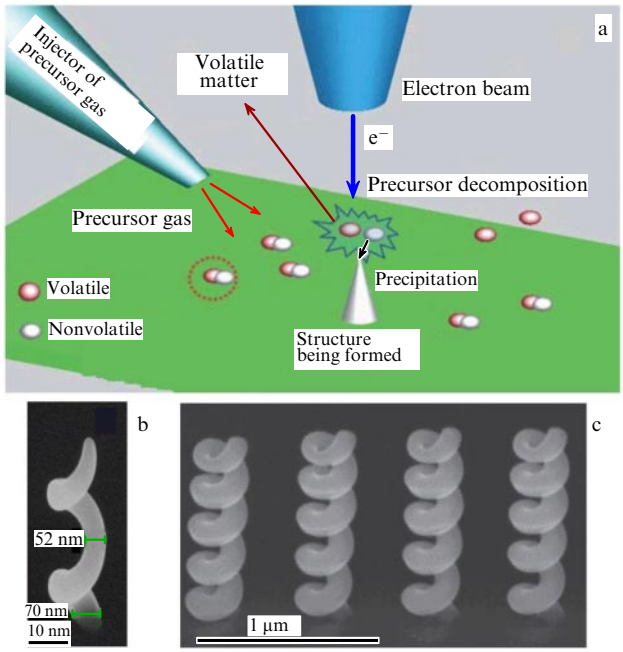

Figure 17. (a) Electron beam-induced gaseous phase deposition [197]. SEM images of nanohelicoides formed by (b) electron [198] and (c) focused ion [199] beams.

The application of atomic force and scanning tunneling microscopes [203–207] to move nanoobjects ensures maximum resolution and permits manipulating individual atoms. The first publications concerning this subject began to appear in the 1990s [208, 209]. Unfortunately, the efficiency of these methods is very low, and they can be used to form structures only on a flat surface. The idea to use a probe to relocate nanoobjects was extended to the concept of a 3D nanoprinter [210]. The proposed device includes a nanomanipulator with a probe having a spatial resolution of up to 40 nm and a 'palette' of a loosely and uniformly distributed initial material (spheres, nanotubes, and other nanostructures), as well as a platform with the substrate moving in three coordinates. Three-dimensional structures are assembled from initial nanoobjects by the manipulator and fixed by laser sintering.

Integration of carbon nanotube synthesis and EHD printing made it possible to develop an original additive method that forms the basis for reaching single-atom resolution in the future. A nanotube fountain pen has been created for 3D manufacturing of metallic nanostructures with a resolution of 10 nm [211]. Metal-encapsulated carbon nanotubes produced by thermal gas-phase deposition are used for the purpose [212]. One of the nanotubes serves as the injector (pen) to deposit material onto the substrate. The injector is fed from a reservoir consisting of a network of carbon nanotubes [213, 214]. Similar to the EHD method, a constant voltage is applied to the injector, functioning as the printhead nozzle (Fig. 18). A continuous mass transfer onto the substrate occurs at 1.5–2.5 V due to electromigration and the temperature gradient of the metal. This approach permitted shaping an 11-nm-wide copper nanowire on the substrate. The authors hope to be able to obtain monoatomic chains encapsulated inside carbon nanotubes [215] with the single-atom resolution of 3D printing [211].

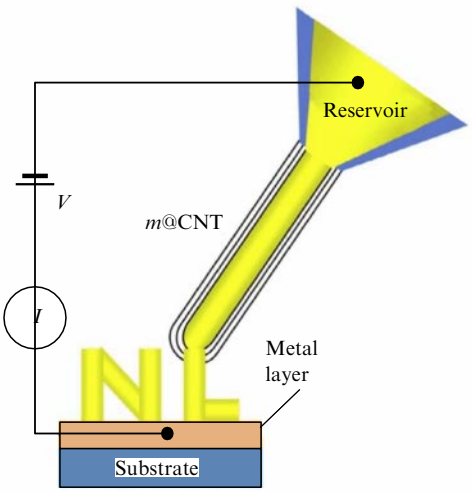

Figure 18. Schematic of device for 3D printing of metals encapsulated inside carbon nanotubes (CNT) [211].

6. Hybrid 3D printing

At present, additive techniques can not yet substitute standard methods. One of the main tasks facing the further development of 3D printing is combining the advantages of various techniques of additive and conventional manufacturing to obtain a synergistic effect. New hybrid technologies are intended to increase the resolving power of methods for the fabrication of 3D composite and gradient materials with enhanced functionalities, design devices with improved characteristics, and increase the cost-effectiveness of their large-scale production.

Performance enhancement of additive production is possible with the use of multiscale technologies. To produce a composite 3D object with micro- and nanocomponents, methods with different resolving powers are integrated into the technological process. The benefits of such an approach were demonstrated by constructing a microfluid 3D device for biomedical applications [216]. A micro-relief in an SU-8 photopolymeric layer deposited onto an Si substrate was formed by single-photon laser polymerization (Fig. 19a). The microgrooves were filled with a different photopolymer (IJP-Dip), and the nanorelief was shaped with the use of the two-photon polymerization technique (Fig. 19b). The 3D structure thus obtained was used as a template for replication by nanoimprint lithography. In other words, the low-efficiency operation of two-photon polymerization was employed precisely to make a small part of the structure. Thus, nonadditive nanoimprint lithography plays the role of a powerful amplifier of the hybrid technology potential facilitating transition to large-scale production.

A hybrid method combining aerosol jet printing and single-photon microstereolithography is described in [217]. It ensures a vertical resolution higher than in microstereolithography and makes it possible to shape structures on a curvilinear surface. First, a photopolymer layer is deposited by inkjet printing process onto the specimen surface (Fig. 19c). Then, laser beam scanning of the surface is performed in accordance with a computer model of the object to polymerize its selected sites. Horizontal and vertical resolution in this approach is 6 μm and 600 nm, respectively.

Hybrid technologies based on a combination of 2D and 3D nanoprinting are described in [218]. They allow integrating the advantages of stereolithography to fabricate intricately shaped 3D structures and of nanoimprint lithography to make films with a nanorelief. Figure 20a compares the standard projection stereolithography technique and two hybrid methods combining the potential of stereolithography and stamp nanolithography (Figs 20b, c). In the former method (Fig. 20b), illumination of each layer produces an imprint of a transparent nanostamp placed at the bottom of a bath. In the latter technique (Fig. 20c), polymeric films obtained by nanoimprint lithography are sequentially integrated into the 3D object during the printing process. The structured film is attached to the polymeric layer thus formed, after which the next one is prepared.

3D printing can be used to create a composite platform for the integration of a few interacting electromagnetic objects, such as chiral meta-materials, waveguides, and Fabry–Pérot resonators, into a single system [219].

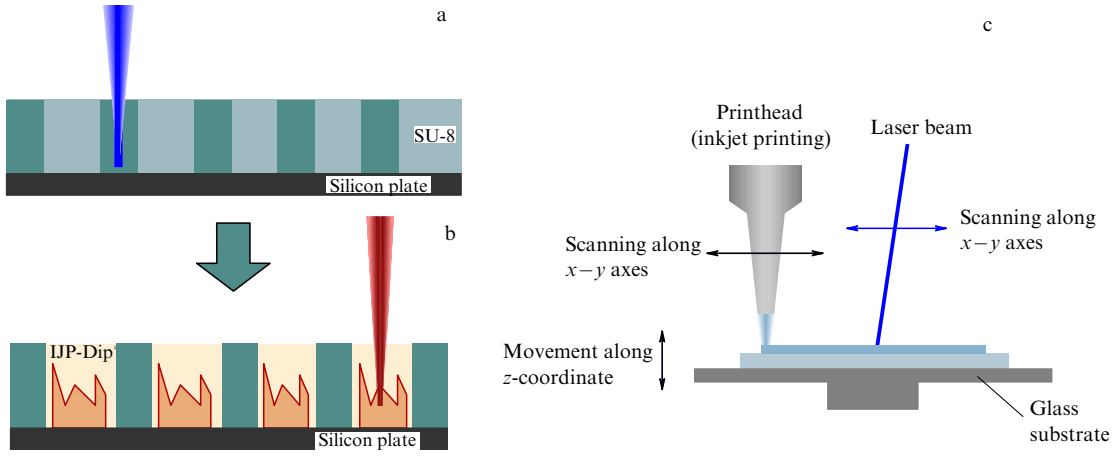

Figure 19. (a, b). Construction of a micro-fluid device by multiscale laser stereolithography. Micro-relief in the SU-8 photoresist layer on an Si substrate is formed by single-photon laser polymerization. After development, the structure obtained is filled with an IJP-Dip photoresist, in which a nanorelief is created by two-photon polymerization [216]. (c) The hybrid method combining inkjet printing and single-photon micro-stereolithography. Inkjet printing is used to deposit a photopolymer layer on the specimen surface. A laser beam causes polymerization of the target area [217].

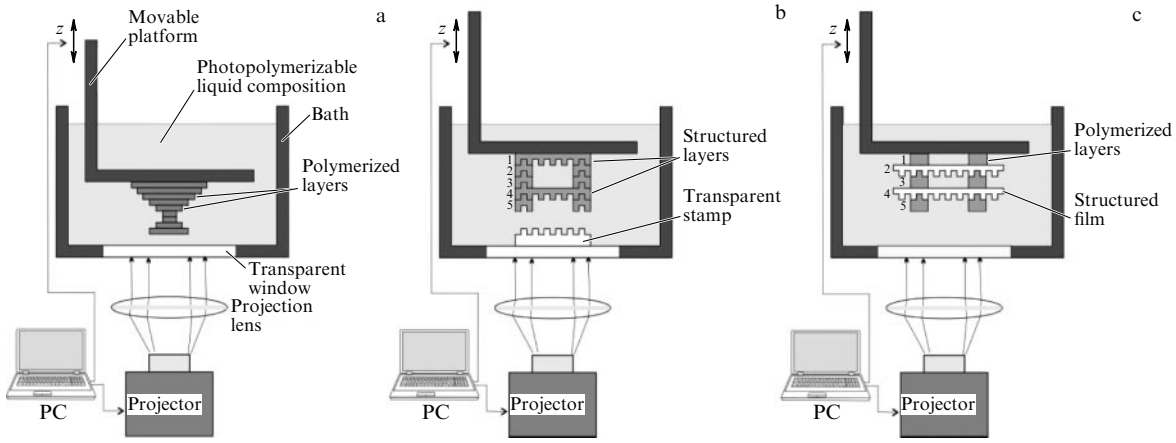

Figure 20. (a) Standard projection stereolithography. (b) Hybrid projection stereolithography — stamp nanolithography with the use of a transparent nanostructured stamp built into the bath bottom. (c) Hybrid method using inbuilt structured polymer films to print a three-dimensional object. A structured polymer film is placed on a polymerized layer of a three-dimensional object prior to formation of the next layer [218].

7. Conclusion

3D printing is a rapidly evolving field of digital technology characterized by the continuous improvement of available and newly emerging additive methods based on the application of an ever increasing variety of physical effects and phenomena.

At the present stage of development of additive technologies, those that have the potential to increase resolution up to the nanometer range and those compatible with high-performance methods or allowing the parallel formation of 3D structures are deemed the most promising. These are single- and two-photon stereolithography as well as laser-induced forward transfer. Other promising techniques include inkjet, especially EHD printing. Nanoimprint lithography and roll-to-roll processing offer powerful tools for the further enhancement of capabilities of additive technologies. Hybrid methods combining the advantages of additive and traditional subtractive techniques are expected to be in high demand in science and technology.

The following main trends in the development of additive technologies can be identified:

(1) Improvement in resolution to nanometer values. Future 3D printing must be based on individual atoms.

(2) Improvement in the quality of objects being formed (reproducibility, surface roughness control, etc.).

(3) Development of new materials for 3D printing with improved functional properties, such as polymers and inks for IJP and LIFT; creation of new composite materials, including those based on nanoparticles and quantum dots.

(4) Enhancement of efficiency of additive technologies and development of parallel 3D printing techniques.

(5) Integration of additive methods into high-performance technologies, e.g., nanoimprint lithography and roll-to-roll processing.

(6) Development of methods for *in situ* control and characterization of manufactured structures.

Taken together, the digital nature of additive technologies and their adaptability to the tasks facing further growth and development in this field, the great variety of methods and materials used accounts for the popularity of 3D printing. Researchers and developers of structures and devices have their own standards and levels of expectation, not infrequently inflated [220, 221]. According to Gartner's predictions [222], 3D printing is now at the peak of expectations. The next stage should be a 5–10 year period of wide practical applications coincident with the time of anticipated revolutionary breakthroughs, including digitalization of manufacturing as the basis for the integration of physical, digital, and biological technologies. 3D printing will be the motivating force of this process. Clearly, micro- and nanoscale applications of 3D printing will not only significantly change photonics, medicine, and electronics but also give rise to new fields, such as the 'internet of things' [223], wearable flexible electronics [224], autonomous multi-sensor platforms [225], lab-on-a-chip and lab-on-fiber technologies [226, 227], and printed bionics [15, 228]. We have attempted to shed some light on the initial stages of this process and the first achievements of 3D printing in the present publication.

The further development of 3D printing is likely to give a powerful impetus to digitalization of manufacturing. Implementation of the 'internet of things' concept will require trillions of various inexpensive 'smart' devices capable of controlling and managing the environment, instruments, buildings, etc. to make the world maximally safe and comfortable for humans [223, 229–231]. 3D printing appears to be a technologically and economically justified option for this purpose in the immediate future.

One more aspect of the development of additive technologies should be mentioned: manufacturing personalization. At some point, the transition from centralized computation to personal computers brought tremendous changes in all spheres of human life. The transition to personalized production outside large industrial centers based on digital models of objects and devices alone and the use of desktop 3D printers may be an equally strong impulse for dramatic innovations in science and technology.

This study was supported by RFBR grant no. 14-29-10261.

References

1. "Standard Terminology for Additive Manufacturing Technologies", ASTM F2792-12a (West Conshohocken, PA: ASTM, 2012) 10.1520/F2792-12A
2. Ren Z, Gao P-X *Nanoscale* **6** 9366 (2014)

3. Prinz V Ya, in *Advances in Semiconductor Nanostructures* (Eds A V Dvurechenskii, A L Aseev) (Amsterdam: Elsevier, 2017) p. 463
4. Prinz V Ya et al. *Physica E* **6** 828 (2000)
5. Prinz V Ya et al. *Sci. Technol. Adv. Mater.* **10** 034502 (2009)
6. Bandyopadhyay A, Bose S (Eds) *Additive Manufacturing* (Boca Raton: CRC Press, 2015)
7. Gibson I, Rosen D, Stucker B *Additive Manufacturing Technologies: 3D Printing, Rapid Prototyping and Direct Digital Manufacturing* (New York: Springer, 2015)
8. Magdassi S, Kamyshny A *Nanomaterials for 2D and 3D Printing* (New York: Wiley-VCH, 2017)
9. Turner M D et al. *Nature Photon.* **7** 801 (2013)
10. Gissibl T et al. *Nature Photon.* **10** 554 (2016)
11. Kong Y L et al. *Nano Lett.* **14** 7017 (2014)
12. Murphy S V, Atala A *Nature Biotech.* **32** 773 (2014)
13. Zhang Y S et al. *Ann. Biomed. Eng.* **45** 148 (2016)
14. Duan B *Ann. Biomed. Eng.* **45** 195 (2017)
15. Mannoor M S et al. *Nano Lett.* **13** 2634 (2013)
16. Hull C W, U.S. Patent No. 4575330A (1986)
17. Bártolo P J *Stereolithography: Materials, Processes and Applications* (New York: Springer, 2011)
18. O'Neill P F et al. *Biomicrofluidics* **8** 052112 (2014)
19. Zhou C et al., in *Proc. of the Annual Solid Freeform Fabrication Symp., Austin, TX, 2011*, p. 65
20. Zhou C et al. *Rapid Prototype. J.* **19** 153 (2013)
21. Pan Y et al., in *Proc. of the ASME 2012 Intern. Manufacturing Science and Engineering* (New York: American Society of Mechanical Engineers, 2012) p. 405
22. Gibson I, Rosen D W, Stucker B *Additive Manufacturing Technologies. Rapid Prototyping to Direct Digital Manufacturing* (London: Springer, 2010)
23. Chatani S, Kloxin C J, Bowman C N *Polymer Chem.* **5** 2187 (2014)
24. Odian G *Principles of Polymerization* (New York: McGraw-Hill, 1970); Translated into Russian: *Osnovy Polimernoi Khimii* (Moscow: Mir, 1974)
25. Mueller J B et al. *Adv. Mater.* **26** 6566 (2014)
26. Andrzejewska E et al. *Phys. Chem. Chem. Phys.* **5** 2635 (2003)
27. Abbe E *Archiv mikroskop. Anatomie* **9** 413 (1873)
28. Maruo S, Nakamura O, Kawata S *Opt. Lett.* **22** 132 (1997)
29. Sugioka K, Cheng Y *Ultrafast Laser Processing: From Micro- to Nanoscale* (Singapore: Pan Stanford, 2013)
30. Sugioka K, Cheng Y *Appl. Phys. Rev.* **1** 041303 (2014)
31. Röhrig M et al. *Small* **8** 3009 (2012)
32. Deubel M et al. *Nature Mater.* **3** 444 (2004)
33. Kawata S et al. *Nature* **412** 697 (2001)
34. Zhou X, Hou Y, Lin J *AIP Adv.* **5** 030701 (2015)
35. Malinauskas M et al. *Lithuanian J. Phys.* **52** 312 (2012)
36. Bückmann T et al. *Adv. Mater.* **24** 2710 (2012)
37. Barton J H et al. *IEEE Trans. Antennas Propagation* **62** 3652 (2014)
38. Barton J H et al. *Prog. Electromagn. Res. B* **41** 269 (2012)
39. Digaum J L et al. *Opt. Express* **22** 25788 (2014)
40. Williams H E et al. *Opt. Express* **19** 22910 (2011)
41. Haske W et al. *Opt. Express* **15** 3426 (2007)
42. Gissibl T et al. *Nature Commun.* **7** 11763 (2016)
43. Grossmann T et al. *Opt. Express* **19** 11451 (2011)
44. Malinauskas M et al. *J. Opt.* **12** 124010 (2010)
45. Rekčytė S et al. *Opt. Express* **21** 17028 (2013)
46. Raimondi M et al. *Micromachines* **5** 341 (2014)
47. Malinauskas M et al. *Micromachines* **5** 839 (2014)
48. Herkommer A M *J. Opt.* **43** 261 (2014)
49. Liberale C et al. *IEEE Photon. Technol. Lett.* **22** 474 (2010)
50. Malinauskas M et al. *J. Opt.* **12** 035204 (2010)
51. Žukauskas A et al. *J. Laser Micro Nanoeng.* **9** 68 (2014)
52. Gissibl T, Schmid M, Giessen H *Optica* **3** 448 (2016)
53. Lindenmann N et al. *Opt. Express* **20** 17667 (2012)
54. Žukauskas A et al. *Proc. SPIE* **8428** 84280K (2012)
55. Xing J-F et al. *Appl. Phys. Lett.* **90** 131106 (2007)
56. Pikulin A, Bityurin N *Phys. Rev. B* **75** 195430 (2007)
57. Pikulin A V, Bityurin N M *Tech. Phys.* **57** 697 (2012); *Zh. Tekh. Fiz.* **82** (5) 120 (2012)
58. Klar T A, Wollhofen R, Jacak J *Phys. Scripta* **2014** 014049 (2014)
59. Fischer J, Wegener M *Laser Photon. Rev.* **7** 22 (2013)
60. Scott T F et al. *Science* **324** 913 (2009)
61. Harke B et al. *Adv. Mater.* **25** 904 (2013)
62. Fischer J, Wegener M *Opt. Mater. Express* **1** 614 (2011)
63. Wolf T J A et al. *Opt. Lett.* **36** 3188 (2011)
64. Andrew T L, Tsai H-Y, Menon R *Science* **324** 917 (2009)
65. Cantu P, Andrew T L, Menon R *Appl. Phys. Lett.* **105** 193105 (2014)
66. Cantu P et al. *Appl. Phys. Lett.* **100** 183103 (2012)
67. Majumder A et al. *AIP Adv.* **6** 065312 (2016)
68. Menon R, Smith H I *J. Opt. Soc. Am. A* **23** 2290 (2006)
69. Sakellari I et al. *ACS Nano* **6** 2302 (2012)
70. Maruo S, Ikuta K *Appl. Phys. Lett.* **76** 2656 (2000)
71. Thiel M et al. *Appl. Phys. Lett.* **97** 221102 (2010)
72. Fischer J et al. *Opt. Express* **21** 26244 (2013)
73. Malinauskas M, Danilevičius P, Juodkazis S *Opt. Express* **19** 5602 (2011)
74. Baldacchini T, Snider S, Zadoyan R *Opt. Express* **20** 29890 (2012)
75. Fischer J, von Freymann G, Wegener M *Adv. Mater.* **22** 3578 (2010)
76. Nielson R, Kaehr B, Shear J B *Small* **5** 120 (2009)
77. Ritschdorff E T, Nielson R, Shear J B *Lab Chip* **12** 867 (2012)
78. Dong X-Z, Zhao Z-S, Duan X-M *Appl. Phys. Lett.* **91** 124103 (2007)
79. Kato J et al. *Appl. Phys. Lett.* **86** 044102 (2005)
80. Salter P S, Booth M J *Opt. Lett.* **36** 2302 (2011)
81. Formanek F et al. *Opt. Express* **14** 800 (2006)
82. Stankevicius E et al. *J. Micromech. Microeng.* **22** 065022 (2012)
83. Smith H I et al. *J. Phys. Conf. Ser.* **415** 012037 (2013)
84. Matsuo S, Juodkazis S, Misawa H *Appl. Phys. A* **80** 683 (2005)
85. Hasegawa S, Hayasaki Y *Opt. Express* **21** 12987 (2013)
86. Hayasaki Y et al. *Appl. Phys. Lett.* **87** 031101 (2005)
87. Takahashi H et al. *Opt. Express* **16** 16592 (2008)
88. Vizsnyiczai G, Kelemen L, Ormos P *Opt. Express* **22** 24217 (2014)
89. Yang L et al. *Opt. Lasers Eng.* **70** 26 (2015)
90. Obata K et al. *Opt. Express* **18** 17193 (2010)
91. Kuang Z et al. *Appl. Surf. Sci.* **255** 2284 (2008)
92. Tumbleston J R et al. *Science* **347** 1349 (2015)
93. Derby B *Annu. Rev. Mater. Res.* **40** 395 (2010)
94. Suganuma K *Introduction to Printed Electronics* (New York: Springer, 2014)
95. de Gans B-J, Duineveld P C, Schubert U S *Adv. Mater.* **16** 203 (2004)
96. Fuh J et al., in *Handbook of Manufacturing Engineering and Technology* (Ed. A Y C Nee) (London: Springer-Verlag, 2015) p. 2567
97. Antonova I V *Phys. Usp.* **60** 204 (2017); *Usp. Fiz. Nauk* **187** 220 (2017)
98. Kamyshny A, Steinke J, Magdassi S *Open Appl. Phys. J.* **4** 19 (2011)
99. Magdassi S *The Chemistry of Inkjet Inks* (Singapore: World Scientific, 2010)
100. Smith P J et al., in *Inkjet-Based Micromanufacturing* (Advanced Micro and Nanosystems, Vol. 9, Eds J G Korvink, P J Smith, D-Y Shin) (Weinheim: Wiley-VCH, 2012)
101. Brand O et al., in *Inkjet-Based Micromanufacturing* (Advanced Micro and Nanosystems, Vol. 9, Eds J G Korvink, P J Smith, D-Y Shin) (Weinheim: Wiley-VCH, 2012)
102. Gan H Y et al. *J. Micromech. Microeng.* **19** 055010 (2009)
103. Ikegawa M, Azuma H *JSME Int. J. B* **47** 490 (2004)
104. Fromm J E *IBM J. Res. Development* **28** 322 (1984)
105. McKinley G H *Rheology Bull.* **74** 6 (2005)
106. Popov Yu O *Phys. Rev. E* **71** 036313 (2005)
107. Deegan R D et al. *Nature* **389** 827 (1997)
108. Deegan R D *Phys. Rev. E* **61** 475 (2000)
109. Deegan R D et al. *Phys. Rev. E* **62** 756 (2000)
110. Shen X, Ho C-M, Wong T-S *J. Phys. Chem. B* **114** 5269 (2010)
111. Park J, Moon J *Langmuir* **22** 3506 (2006)
112. de Gans B-J, Schubert U S *Langmuir* **20** 7789 (2004)
113. Lim J A et al. *Adv. Function. Mater.* **18** 229 (2008)
114. Kajiya T et al. *J. Phys. Chem. B* **113** 15460 (2009)
115. Prinz A V, Prinz V Ya, Seleznev V A *Microelectron. Eng.* **67–68** 782 (2003)
116. Ahn B Y et al. *Science* **323** 1590 (2009)
117. Noh Y-Y et al. *Nature Nanotechnol.* **2** 784 (2007)
118. Zhao N et al. *J. Appl. Phys.* **101** 064513 (2007)
119. Kullmann C et al. *J. Micromech. Microeng.* **22** 055022 (2012)
120. Kamyshny A, Magdassi S *Small* **10** 3515 (2014)
121. Nebogatikova N A et al. *Phys. Chem. Chem. Phys.* **17** 13257 (2015)

122. Perelaer J et al. *Adv. Mater.* **21** 4830 (2009)
123. Perelaer J et al. *Adv. Mater.* **24** 2620 (2012)
124. Ko S H et al. *Appl. Phys. Lett.* **90** 141103 (2007)
125. Kang H, Sowade E, Baumann R R *ACS Appl. Mater. Interfaces* **6** 1682 (2014)
126. Allen M L et al. *Nanotechnology* **19** 175201 (2008)
127. Reinhold I et al. *J. Mater. Chem.* **19** 3384 (2009)
128. Grouchko M et al. *ACS Nano* **5** 3354 (2011)
129. Reiser B et al. *Chem. Sci.* **7** 4190 (2016)
130. Park J-U et al. *Nature Mater.* **6** 782 (2007)
131. Park J-U et al. *Nano Lett.* **10** 584 (2010)
132. Onses M S et al. *Small* **11** 4237 (2015)
133. Zheng G et al. "Direct-write micro/nano-structure for flexible electronic manufacturing", in *7th IEEE Conf. on Nanotechnology, IEEE NANO, 2–5 August 2007*, https://doi.org/10.1109/NANO.2007.4601304
134. Taylor G, Van Dyke M D *Proc. R. Soc. Lond. A* **313** 453 (1969)
135. Dalton P D et al. *Biomater. Sci.* **1** 171 (2013)
136. Brown N A, Gladstone J N, Chiarot P R *J. Micro Nano-Manuf.* **3** 014502 (2015)
137. An B W et al. *Adv. Mater.* **27** 4322 (2015)
138. Richner P et al. *ACS Photon.* **3** 754 (2016)
139. Galliker P et al. *Nature Commun.* **3** 890 (2012)
140. Schneider J et al. *Adv. Function. Mater.* **26** 833 (2016)
141. Han Y, Wei C, Dong J *Manufact. Lett.* **2** 96 (2014)
142. Hansen C J et al. *Adv. Mater.* **25** 96 (2013)
143. Sutanto E et al. *J. Micromech. Microeng.* **22** 045008 (2012)
144. Sutanto E et al. *Manufact. Lett.* **2** 4 (2014)
145. Lee J-S et al. *Appl. Phys. Lett.* **93** 243114 (2008)
146. Lee K I et al., in *Proc. of the IEEE 26th Intern. Conf. on Micro Electro Mechanical Systems, MEMS 2013, January 20–24, 2013, Taipei, Taiwan* (Piscataway, NJ: IEEE, 2013) p. 1165
147. Coppola S et al. *Proc. SPIE* **9705** 97050L (2016)
148. Ferraro P et al. *Nature Nanotechnol.* **5** 429 (2010)
149. Vespini V et al. *Lab Chip* **16** 326 (2016)
150. de Angelis M et al. *Appl. Phys. Lett.* **103** 163112 (2013)
151. Tagawa Y et al. *Phys. Rev. X* **2** 031002 (2012)
152. Moser C et al. *Proc. SPIE* **9764** 97641D (2016)
153. Kim J T et al. *ACS Macro Lett.* **1** 375 (2012)
154. Kim J T et al. *Adv. Mater.* **23** 1968 (2011)
155. Jung S et al. *Adv. Energy Mater.* **4** 1400432 (2014)
156. Azzellino G et al. *Adv. Mater.* **25** 6829 (2013)
157. Fukuda K et al. *Nature Commun.* **5** 4147 (2014)
158. Xu W et al. *Adv. Mater.* **28** 527 (2016)
159. Blattmann M et al. *Opt. Express* **23** 24525 (2015)
160. Chen W-C et al. *J. Micromech. Microeng.* **23** 065008 (2013)
161. Liu X et al. *Nature Commun.* **5** 4007 (2014)
162. Sutanto E, Alleyne A *Mechatronics* **31** 243 (2015)
163. Søndergaard R R, Hösel M, Krebs F C *J. Polymer Sci. B* **51** 16 (2013)
164. Visser C W et al. *Adv. Mater.* **27** 4087 (2015)
165. Wang J et al. *Adv. Mater.* **22** 4462 (2010)
166. Zenou M, Kotler Z *Opt. Express* **24** 1431 (2016)
167. Banks D P et al. *Appl. Phys. Lett.* **89** 193107 (2006)
168. 't Veld B H et al. *CIRP Ann.* **64** 701 (2015)
169. Wu P K et al. *Thin Solid Films* **398–399** 607 (2001)
170. Arnold C et al. *Laser Focus World* **40** S9 (2004)
171. Pique A et al. *Proc. SPIE* **5662** 564 (2004)
172. Munoz-Martin D et al. *Appl. Surf. Sci.* **366** 389 (2016)
173. Willis D A, Grosu V *Appl. Phys. Lett.* **86** 244103 (2005)
174. Sametoglu V, Sauer V T K, Tsui Y Y *Opt. Express* **21** 18525 (2013)
175. Hennig G et al. *J. Laser Micro Nanoeng.* **7** 289 (2012)
176. Sridhar A et al., in *Proc. of the IEEE 62nd Electronic Components and Technology Conf., San Diego, CA, USA* (Piscataway, NJ: IEEE, 2012) p. 238
177. Nguyen A K, Narayan R J *Ann. Biomed. Eng.* **45** 84 (2017)
178. Arnold C B, Serra P, Piqué A *MRS Bull.* **32** 23 (2007)
179. Constantinescu C et al. *Appl. Surf. Sci.* **374** 49 (2016)
180. Nagel M et al. *Appl. Phys. A* **92** 781 (2008)
181. Shaw-Stewart J et al. *Appl. Surf. Sci.* **258** 9309 (2012)
182. Brown M S et al. *J. Fluid Mech.* **709** 341 (2012)
183. Kattamis N T, Brown M S, Arnold C B *J. Mater. Res.* **26** 2438 (2011)
184. Kuznetsov A I, Koch J, Chichkov B N *Opt. Express* **17** 18820 (2009)
185. Korte F, Koch J, Chichkov B N *Appl. Phys. A* **79** 879 (2004)
186. Makrygianni M et al. *Appl. Surf. Sci.* **297** 40 (2014)
187. Zywietz U et al. *Appl. Phys. A* **114** 45 (2014)
188. Zywietz U et al. *Nature Commun.* **5** 3402 (2014)
189. Feinaeugle M et al. *Appl. Phys. A* **122** 398 (2016)
190. Auyeung R C Y et al. *Appl. Phys. A* **102** 21 (2011)
191. Auyeung R C Y et al. *Opt. Express* **23** 422 (2015)
192. Piqué A et al. *Proc. SPIE* **8608** 86080K (2013)
193. Dong L, Arai F, Fukuda T *Appl. Phys. Lett.* **81** 1919 (2002)
194. Madsen D N et al. *Nano Lett.* **3** 47 (2003)
195. Yokota T, Murayama M, Howe J M *Phys. Rev. Lett.* **91** 265504 (2003)
196. Xu S et al. *Small* **1** 1221 (2005)
197. De Angelis F et al. *Nanoscale* **3** 2689 (2011)
198. Esposito M et al. *ACS Photon.* **2** 105 (2015)
199. Esposito M et al. *Adv. Opt. Mater.* **2** 154 (2014)
200. Jesse S et al. *ACS Nano* **10** 5600 (2016)
201. Sezen M, in *Modern Electron Microscopy in Physical and Life Sciences* (Ed. M Janecek) (London: IntechOpen, 2016) p. 1624
202. Vaezi M, Seitz S, Yang S *Int. J. Adv. Manufact. Technol.* **67** 1721 (2013)
203. Sugimoto Y et al. *Nature Mater.* **4** 156 (2005)
204. Custance O, Perez R, Morita S *Nature Nanotechnol.* **4** 803 (2009)
205. Gohlke D et al. *Nano Lett.* **13** 2418 (2013)
206. Olyanich D A et al. *Nanotechnology* **24** 055302 (2013)
207. Morgenstern K, Lorente N, Rieder K-H *Phys. Status Solidi B* **250** 1671 (2013)
208. Eigler D M, Schweizer E K *Nature* **344** 524 (1990)
209. Junno T et al. *Appl. Phys. Lett.* **66** 3627 (1995)
210. Carlson M B et al. *3D Print. Additive Manufact.* **2** 123 (2015)
211. Fan Z et al. *Carbon* **86** 280 (2015)
212. Tao X Y et al. *Diamond Related Mater.* **15** 1271 (2006)
213. Dong L et al. *Nano Lett.* **9** 210 (2009)
214. Dong L et al. *IEEE Nanotechnol. Mag.* **4** 13 (2010)
215. Kitaura R et al. *Angew. Chem. Int. Ed.* **48** 8298 (2009)
216. Hengsbach S, Lantada A D *Biomed. Microdev.* **16** 617 (2014)
217. Obata K et al. *J. Laser Micro Nanoeng.* **9** 242 (2014)
218. Seleznev V A, Prinz V Ya *Nanotechnology* **28** 064004 (2017)
219. Prinz V Ya et al. *Sci. Rep.* **7** 43334 (2017)
220. Huang Y et al. *J. Manuf. Sci. Eng.* **137** 014001 (2015)
221. Dezhina I G et al. *Novye Proizvodstvennye Tekhnologii. Publichnyi Analiticheskii Doklad* (Public Analytical Report on Development of New Production Technologies) (Moscow: Delo, 2015)
222. Shanler M, Basiliere P "Hype Cycle for 3D Printing, 2015", Accessed 01.04.17, 2017, https://www.gartner.com/doc/3100228
223. Ortiz A M et al. *IEEE Internet Things J.* **1** 206 (2014)
224. Park M et al. *Adv. Healthcare Mater.* **4** 991 (2015)
225. Honda W et al. *Adv. Funct. Mater.* **24** 3299 (2014)
226. Yazdi A A et al. *Microfluid. Nanofluid.* **20** 50 (2016)
227. Cusano A et al. (Eds) *Lab-on-Fiber Technology* (Wiesbaden: Springer, 2015)
228. Kong Y L et al. *Nano Today* **11** 330 (2016)
229. Xu L D, He W, Li S *IEEE Trans. Industrial Inform.* **10** 2233 (2014)
230. Rosa P, Câmara A, Gouveia C *Open J. Internet Things* **1** 16 (2015)
231. Whitmore A, Agarwal A, Xu L D *Inf. Syst. Front.* **17** 261 (2015)